Laporan Akhir Projek Penyelidikan Jangka Pendek

Synthesize of Nanoporous Ceramic Membrane with Bimodal Pore Size Distribution Using Nanosized Template

by
Prof. Dr. Abdul Latif Ahmad
Dr. Syamsul Rizal Abd. Shukor

2008

Rem

LAPORAN AKHIR PROJEK PENYELIDIKAN JANGKA *PENDEK*
FINAL REPORT OF SHORT TERM RESEARCH PROJECT
Sila kemukakan laporan akhir ini melalui Jawatankuasa Penyelidikan di Pusat
Pengajian dan Dekan/Pengarah/Ketua Jabatan kepada Pejabat Pelantar Penyelidikan

UNIVERSITI SAINS MALAYSIA

1. **Nama Ketua Penyelidik: Abdul Latif Ahmad**
   Name of Research Leader

   [√] Profesor / *Prof.*   [ ] Dr./ *Dr.*   [ ] Encik/Puan/Cik *Mr/Mrs/Ms*

2. **Pusat Tanggungjawab (PTJ): Pusat Pengajian Kejuruteraan Kimia**
   School/Department
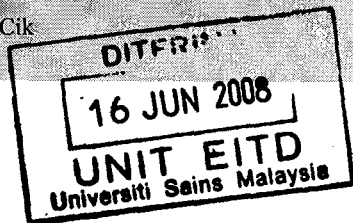
3. **Nama Penyelidik Bersama: Dr. Syamsul Rizal Abd. Shukor**
   Name of Co-Researcher

4. **Tajuk Projek:** **Synthesize of Nanoporous Ceramic Membrane with Bimodal Pore Size**
   Title of Project

   Distribution Using Nanosized Template

5. **Ringkasan Penilaian/*Summary of Assessment*:**

	Tidak Mencukupi *Inadequate* 1	2	Boleh Diterima *Acceptable* 3	Sangat Baik *Very Good* 4	5
i) Pencapaian objektif projek: *Achievement of project objectives*			√		
ii) Kualiti output: *Quality of outputs*				√	
iii) Kualiti impak: *Quality of impacts*				√	
iv) Pemindahan teknologi/potensi pengkomersialan: *Technology transfer/commercialization potential*			√		
v) Kualiti dan usahasama : *Quality and intensity of collaboration*			√		
vi) Penilaian kepentingan secara keseluruhan: *Overall assessment of benefits*			√		

1

6. **Abstrak Penyelidikan**
   (Perlu disediakan di antara 100 - 200 perkataan di dalam **Bahasa Malaysia dan juga Bahasa Inggeris**. Abstrak ini akan dimuatkan dalam Laporan Tahunan Bahagian Penyelidikan & Inovasi sebagai satu cara untuk menyampaikan dapatan projek tuan/puan kepada pihak Universiti & masyarakat luar).

   Abstract of Research
   (An abstract of between 100 and 200 words must be prepared in Bahasa Malaysia and in English).
   This abstract will be included in the Annual Report of the Research and Innovation Section at a later date as a means of presenting the project findings of the researcher/s to the University and the community at large)

   Please refer to Appendix A

7. **Sila sediakan laporan teknikal lengkap yang menerangkan keseluruhan projek ini.**
   [Sila gunakan kertas berasingan]
   Applicant are required to prepare a Comprehensive Technical Report explaning the project.
   (This report must be appended separately)
   Please refer to Appendix B

   Senaraikan kata kunci yang mencerminkan penyelidikan anda:
   List the key words that reflects your research:

Bahasa Malaysia	*Bahasa Inggeris*

8. **Output dan Faedah Projek**
   Output and Benefits of Project

   (a) * **Penerbitan Jurnal**
   Publication of Journals
   (Sila nyatakan jenis, tajuk, pengarang/editor, tahun terbitan dan di mana telah diterbit/diserahkan)
   (State type, title, author/editor, publication year and where it has been published/submitted)

   Please refer to Appendix C

(b)   **Faedah-faedah lain seperti perkembangan produk, pengkomersialan produk/pendaftaran paten atau impak kepada dasar dan masyarakat.**
State other benefits such as product development, product commercialisation/patent registration or impact on source and society.

Ahmad, A.L., Abd. Shukor, S.R., Leo, C.P. (2007) γ-Alumina with Bimodal Pore Size Distribution:

Transport Resistance Diminution in Bi-Layered Membrane. International Exposition of Research and

Inventions of Institutions of Higher Learning 2007, **Gold Prize**, Kuala Lumpur.

* Sila berikan salinan/*Kindly provide copies*

(c)   **Latihan Sumber Manusia**
Training in Human Resources

i)   Pelajar Sarjana: 1
Graduates Students
(Perincikan nama, ijazah dan status)
(Provide names, degrees and status)

Leo Choe Peng (PJ-D0028), calon penuh masa untuk Ijazah Doktor Falsafah

Calon ini telah hantar sepuluh salinan tesis.

ii)   Lain-lain:
Others

9.   **Peralatan yang Telah Dibeli:**
Equipment that has been purchased

1.   Regulator

2.   Dead-end filtration system

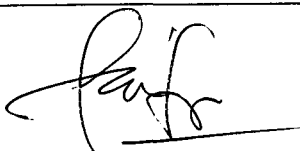|	
~~Latuj~~	✗
Tandatangan Penyelidik	**Tarikh**
Signature of Researcher	*Date*

3/6/08

3

Komen Jawatankuasa Penyelidikan Pusat Pengajian/Pusat
Comments by the Research Committees of Schools/Centres

Projek ini telah berjaya dan tamat mengikut objektif asal seperti dalam cadangan asal

10/06/08

DR. SYAMSUL RIZAL ABD. SHUKOR
Timbalan Dekan
(Akademik & Pembangunan Pelajar)
b.p. Dekan

TANDATANGAN PENGERUSI **JAWATANKUASA PENYELIDIKAN** **PUSAT PENGAJIAN/PUSAT** *Signature of Chairman* *[Research Committee of School/Centre]*	**Tarikh** *Date*

4

APPENDIX A

Abstrak

Walaupun membran seramik mempunyai rintangan yang tinggi terhadap haba dan bahan kimia, kebolehtelapannya adalah lebih rendah berbanding dengan membran organik. Selain daripada mengurangkan ketebalan membran yang akan menyebabkan kecacatan, membran seramik dioptimumkan dalam kajian ini dengan memperkenalkan membran seramik berliang dwimod yang dipencontohkan dengan sfera polistirena bersaiz nano. Dalam membran silika/γ-alumina, lapisan γ-alumina berliang dwimod digunakan sebagai lapisan pertengahan dengan berjaya untuk mengurangkan rintangan pengankutan. Untuk membina γ-alumina berliang diwmod, sfera polistirena (diameter $\approx$ 50 nm) ditambahkan ke dalam sol boehmit. Sol mempamerkan aspek yang berlainan dalam kehilangan berat dan kelikatan. Selepas dikalsin pada 500 °C untuk 1 jam, pencontoh disingkirkan dengan pengecutan liang yang kecil. Untuk 20 ml sol boehmit, kuantiti pencontoh kurang daripada 0.5 g dicadangkan untuk mencipta liang-liang sekundar tersusun. Dengan mengguna kaedah pencirian penjerapan/penyaherapan N_2, sampel γ-alumina yang dioptimumkan menunjukkan diameter liang primer 5 – 6 nm dengan isipadu liang sekunder yang agak rendah. Digunakan sebagai lapisan pertengahan, membran γ-alumina berliang dwimod banyak mengurangkan rintangan pengangkutan membran dwi-lapis. Rintangan spesifik lapisan silika dikurangkan hampir 62 % apabila disokong atas lapisan γ-alumina berliang dwimod yang dioptimumkan. Kaedah gerak balas permukaan dengan rekabentuk pusat komposit dijalankan untuk mengkaji pengaruh keadaan operasi umum ke atas kualiti dan kuantiti telapan apabila membran silika/g-alumina dengan lapisan pertengahan berliang dwimod yang dioptimumkan diaplikasikan dalam penapisan-nano campuran pewarna-garam-air. Penolakan perwarna dicapai lebih tinggi daripada 90 %. Model mencadangkan penahanan garam dipengaruhi oleh tekanan, kepekatan suapan pewarna dan garam. Akan tetapi, fluks telapan merosot disebabkan pengutuban kepekatan dan kekotoran.

Abstract

Although ceramic membranes possess great resistance toward heat and chemicals, the permeability of ceramic membranes is relatively low compared to organic membranes. Instead of reducing membrane thickness which induces defects; the ceramic membrane was optimized in this study by introducing bimodal porous ceramic membrane templated by nanosized polystyrene spheres. In silica/γ-alumina membrane, bimodal porous γ-alumina layer was successfully utilized as intermediate layer in order to reduce transport resistance. For tailoring bimodal porous γ-alumina, polystyrene spheres (diameter $\approx$ 50 nm) were added into boehmite sol. The sol exhibited fairly different aspect in weight loss and viscosity. After calcined at 500 ^{o}C for 1 hr, template was removed with small pore shrinkage. For 20 ml boehmite sol, template quantity less than 0.5 g was recommended for creating ordered secondary pores. Characterized using N_2 adsorption/desorption, the optimized γ-alumina samples showed primary pore diameter of 5 - 6 nm with relatively low secondary pore volume. Utilized as intermediate layer, bimodal porous γ-alumina membrane reduced the transport resistance of bi-layered ceramic membrane greatly. Specific resistance of silica layer reduced nearly 62 % when supported on the optimized bimodal porous γ-alumina layer. Response surface method with central composite design was performed to study the influence of common operating conditions on the quality and quantity of permeate when the optimized silica/γ-alumina membrane with bimodal porous intermediate layer was applied in the nanofiltration of dye-salt-water mixture. The rejection of dye achieved more than 90 %. The model suggested that the salt retention was affected by pressure, the feed concentration of dye and salt. However, the separation was susceptible to flux decline due to concentration polarization and fouling.

APPENDIX B

Comprehensive Technical Report

In overall, the main objectives of the project have been successfully achieved. A porous ceramic membrane with a bimodal pore size distribution has been synthesized and characterized. A simple templating method was used to control secondary pore size and pore order. The separation ability and mass transfer phenomenon of the bimodal porous ceramic membrane was also studied. In the dye-salt-water mixture separation test, the separation ability of the bimodal porous ceramic membrane was optimized in order to achieve high rejection of dye. The following sections report on the results obtained from this research.

1. Introduction

Membrane technology is energy efficient and cost effective. It represents promising alternative to conventional separation methods such as energy-intensive distillation, cryogenic separation and pressure swing adsorption (Baker, 2000). Ceramic membranes have the advantages of thermal stability, solvents and chemicals resistance, sterilization ability and biocompatibility compared to polymeric membranes (Buggraaf and Keizer, 1991). They are not only widely applied in separation and purification, but also in fuel cells and catalytic membrane reactors. Among the ceramics membranes, porous silica membranes have drawn the greatest attention from researchers and technologists. Silica membranes show promising molecular sieving characteristics in gas separation (Uhlhorn et al., 1989). Besides that, silica membranes have been successfully utilized in pervaporation (Sekulic et al., 2004) and electrolyte separation (Samuel de Lint et al., 2006). Porous silica membranes with tunable pore sizes can be processed by simple sol-gel method or chemical vapor deposition (CVD). More importantly, silica membrane can even be templated with orderly arranged mesopores, uniform pores, enormous surface area and high pore volume using surfactant (Lin, 2001).

In general, macroporous supports are coated with an intermediate layer (such as γ-alumina or titania) prior to the deposition of silica membrane. It is difficult to coat silica membrane directly on macroporous supports with pore sizes substantially larger than 50 nm due to occurrence of defects (Tsai et al., 2000). Besides facilitating the deposition of a defect-free overlying silica thin layer, intermediate layer also improves the electrolyte retention at pH values close to iso-electric points (IEP) of separating layer (Samuel de Lint et al., 2006). However, the permeate flux is largely reduced when a bi-layered membrane is utilized. Chowdhury et. al. (2006) demonstrated that intermediate layer contributes significant transport resistance in silica/γ-alumina membrane which reduces the applicability of silica membranes. To further improve permeability of silica/γ-alumina membrane, Tsai et al.(2000) have introduced additional coating of surfactant templated silica between γ-alumina and microporous silica layer. Meanwhile, Yoshino et al. (2005) have introduced fourth layer of α-alumina

which located between the silica/γ-alumina membrane and membrane support. The thickness of the γ-alumina membrane was reduced in the four layers configuration. Apart from creating more hierarchical structure, some researchers such as Lee *et al.* (2005) and So *et al.* (1998) used soaking and vapor-deposition (SVD) method to create thin and uniform membrane as intermediate layer in the porous support. In this study, the permeability of ceramic membrane was improved by introducing bimodal porous intermediate layer templated by nanosized polystyrene beads. Although the preparation of ceramics with a bimodal porous structure is greatly reported, not much work was published on the synthesis of ceramic membranes with a bimodal pore size distribution. Penaa-Alonso *et al.* (2007) only described the preparation of a porous silicon–titanium oxycarbide membrane with a bimodal pore size distribution. Meanwhile, Tsuru *et al.* (2006) synthesized a bimodal porous a-alumina membrane for steam reforming of methane. Owing to the lack of related work, it is important to synthesize thin layers of ceramics with a bimodal pore size distribution and to understand their characteristics in liquid separation tests.

2.   Methodology

2.1   *Preparation of bimodal porous silica/γ-alumina membrane*

In the preparation of γ-alumina, a boehmite sol was synthesized using the sol–gel method described by Lambert and Gonzalez. (1999). Polyethylene glycol, PEG (Merck Company, Malaysia) was added into de-ionized water as a binder; the amount of PEG is 2 wt% of final solution. Aluminum secbutoxide (Fluka, Malaysia) was the sol precursor which allowed open stirring to evaporate butanol at 85 °C for 15 min. Dilute *HCl* (Merck Company, Malaysia) was then added as a peptization agent with the final molar ratios of *Al:H2O: HCl* = 1:100:0.07. The resulting solution was stirred for 16 h at 80 °C in a closed container to form a clear, stable boehmite sol. Later, nanosized polystyrene beads (ca. 50 nm in diameter) were synthesized through emulsion polymerization (Gilbert, 1995). The latex was washed with distilled water using an ultrafiltration membrane and then freeze dried. 0.5 g of nanosized polystyrene eads was added into 20 ml of boehmite sol and stirred overnight. This sample was labeled as A050. Using the same method, sample A025 was prepared by adding 0.25 g nanosized polystyrene beads. Then, alumina supports were dip coated with boehmite sol (labeled as A000), A025 and A050. The porous membrane supports used in this work are α-alumina discs with diameter of 28.0 mm and average thickness of 1 mm. After dip coating, the nanosized polystyrene beads in A025 and A050 were assembled using vacuum iltration force. All dried samples were calcined at 500 °C for 1 h to form γ-alumina with different pore structures. The silica sol synthesis was carried out as reported by Honma *et al.* (2000). In this method, a mixture of tetra-ethoxyorthosilicate (8 ml, Fluka) and 1-propanol (17.5 ml, Fluka) was stirred in a 100 ml flask at 600 rpm for 5 min. *HCl* was then added as hydrolyzing agent (0.33 ml (36 N) *HCl* solution in 2 ml water) and was stirred for 60 min. Co-solvent 2-butanol (8.8 ml, Fluka) was added and was stirred for another 30 min. In the final step, 1.75 g of cetyl-trimethyl-ammonium bromide (Aldrich, Malaysia) was dissolved in 4.5 ml of de-ionized water.

The surfactant solution was poured into the silica solution and the mixture was stirred for 60 min. The sol was then deposited on top of different types of intermediate layers (A000, A050 and A025) and also on the α-alumina support. The silica coated supports were calcined at 450 °C for 90 min in air with heating and cooling rates of 0.2 °C/min.

2.2   Characterization methods

X-ray diffraction (XRD) patterns of the samples A000, A025 and A050 were measured at room temperature using a Philips Goniometer PW1820, diffractometer PW 1710 and X-ray generator PW1729. The phase analysis was done in the range of $10° < 2\theta < 70°$ (A000, A025 and A050) at a wavelength $\lambda = 1.54060$Å. The samples were ground into fine powders before analysis. Then, transmission electron microscopy (TEM) was used to observe the microstructure of A000, A025, A050 and Si (silica). TEM was performed using a Phillips CM12 microscope in the operating voltage range of 15–45 kV. The samples were prepared by allowing a distilled water suspension (A000, A025 and A050) or ethanol suspension (Si) of the finely ground powder to evaporate on a copper grid coated with a holey carbon film. Lastly, scanning electron microscopy (SEM) and energy dispersive X-ray microanalysis (EDX) studies were carried out using Leo Supra 55VP Ultra High Resolution Analytical Field Emission Scanning Electron Microscope with an operating voltage of 15 kV. The alumina supports with different membranes were fractured and attached to a metal mount using carbon tape. Membranes fracture cross sections were coated with gold and placed on aluminum–gold plating for analyses.

2.3   Separation test

Steady-state water permeability measurements were carried out in a dead-end filtration cell with different types of membranes. The operating pressure range was kept in the range of 200–500 kPa. Liquid stirring was done with a magnetic stirrer at a constant stirring speed of 500 rpm throughout the permeation experiments. De-ionized water (18 MΩ cm) was used for determination of membrane permeability. MWCOs of the membranes were determined by using PEG with different molecular weights. In the PEG retention test, PEG solution (50 ppm) was fed in and filtered at 400 kPa. The concentration of PEG in the permeate was determined using methods introduced by Sadbe *et al.* (Sabde *et al.*, 1997). 4 ml of sample solution was added to 1 ml 5% (w/v) $BaCl_2$ in 1 N HCl. To this mixture, 1 ml of solution, prepared by dissolving 1.27 g I_2 in 100 ml 2% KI (w/v) solution was added which is further diluted 10 times. Color was allowed to develop for 15 min at room temperature, and absorption was read using a spectrophotometer at 535 nm against a reagent blank.

The dye separation experiments were conducted using a dead-end filtration cell in the range 4-10 bar. Feed solution concentrations of Reactive Red 120 (RR120), Reactive Black 5 (RB5) and Reactive Orange (RO16) were kept at 250 - 1000 ppm. The bulk solution was stirred at 500 rpm. Feed and permeate concentrations of the dye were measured using UV-Vis Spectrophotometer (Thermo

Spectronic, USA; model GENESYS 2). The wavelengths at which maximum absorption occurred were 530 nm for RR120, 592 nm for RB5 and 493 nm for RO16. The salt retention experiments were performed at 25 ± 1 °C using the same dead-end permeation set-up. The retention experiments were conducted with aqueous solutions of 7.5 mM *NaCl* at various pH. The pH was adjusted using 0.25 M *NaOH* and *HCl*. During each pH experiment permeate samples were collected at a pressure 10 bar. The *NaCl* concentrations were measured using a conductivity meter (Hanna Instruments, Italy, Model: HI9033). A period of 15 min was used to allow both the flux and the permeate retention to reach steady state. During this equilibration period, the permeate conductivity and flux were continuously monitored to assure that a steady-state situation had been reached. In the final stage of the research, response surface method (RSM) with central composite design (CCD) was performed in order to study the influence of common operating conditions on the quality and quantity of permeate when A025/Si membrane was applied in the nanofiltration (NF) of dye-salt-water mixtures.
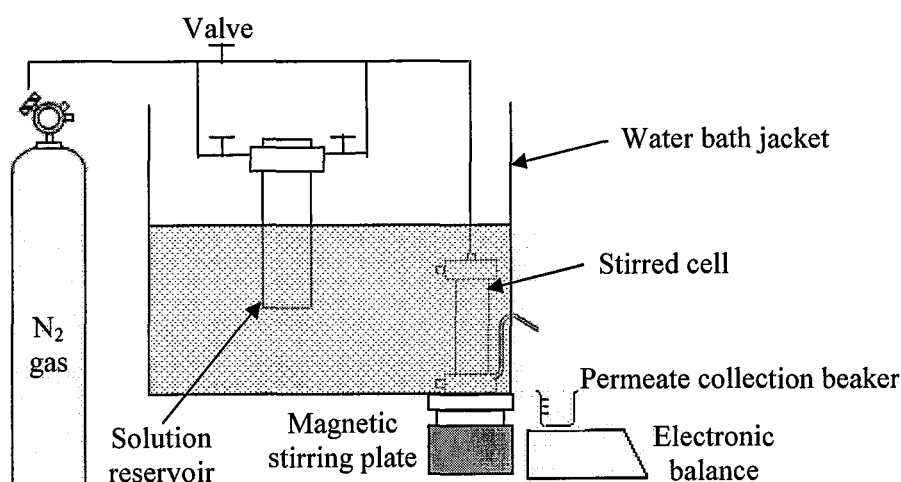

Fig. 1. Filtration system for separation test using ceramic membrane

3.   Results and Discussions

3.1   *Bimodal Porous γ-Alumina: Template, Sol and Calcined Oxide*

This section details the characterization of template, boehmite sol with template and templated γ-alumina. The main objective of this section is to find the optimum quantity of templating units (nanosized PS beads) to be added as well as the best heat treatment conditions to create the secondary pores. This is done by understanding the characteristic changes of sol and calcined product when nanosized PS beads are added and removed in the sol-gel method. The characteristic changes studied include weight loss in relation to temperature changes, viscosity, chemical composition, crystallographic structure and porosity. Characterization methods such as TEM, TGA, viscometer, FT-IR, XRD, N_2 adsorption/desorption are utilized to achieve the mentioned objectives.

TEM picture of a PS bead with diameter ca. 50 nm is shown in Fig. 2. The mean particle size of PS beads is 50 nm with fairly narrow particle size distribution. In summary, the PS beads possess spherical shape and required particle size which are essential for constant templating effect.
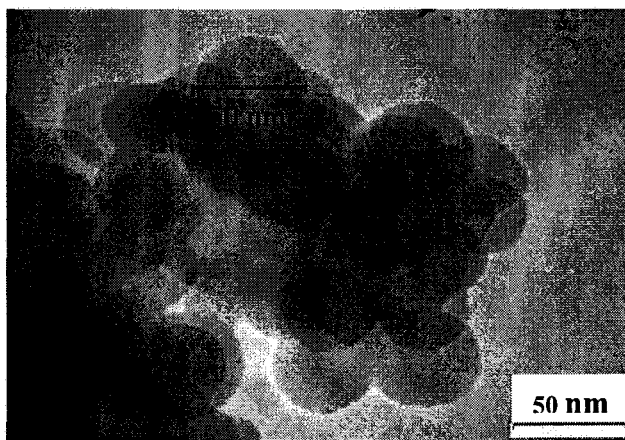

Fig. 2. TEM pictures of nanosized PS beads.

The effect of template on boehmite sol thermal stability is investigated using thermogravimetry method. This part of the study concerns primarily on the changes of weight of dried sols as gradual heating is employed. Based on the observed changes, conclusions are drawn on the determination of suitable calcination conditions in order to remove template and form bimodal porous γ-alumina. The thermogravimetric curves of the fresh A00, A025, A050 and A100 gel are shown on Fig. 3. After addition of template, the gels exhibit a fairly different aspect in weight loss. The total weight loss up to 800 °C of samples A025, A050 and A100 is approximately 44 wt%, 62 wt% and 70 wt% respectively. The weight loss observed is most likely dependent on the amount of PS beads added, with the highest weight loss occurring in A100. Similarly, due to the lower content of PS beads in A025 gel compared to A050 gel, the weight loss observed is lower. However, total weight loss of sample A000 is close to sample A025. It is possible that the water content in sample A000 is higher and leads to obscure difference of total weight loss. The thermogravimetric curves of all samples show

four weight loss events, namely 25 - 100 °C region, 100 - 200 °C region, 200 - 450 °C region and above 450 °C region. The first weight loss in the 25 - 100 °C region can be related to the loss of adsorbed water molecules. Weight loss of samples in the second region 100 - 200 °C corresponds to loss of weakly bound water molecules, coordinated water molecules and interlayer water molecules. For sample A000, the major weight loss event occurs from 200 – 450 °C and it corresponds to dehydration and dehydroxylation of the hydrous aluminium oxide. Above 450 °C, sample A000 still shows continued weight loss that is possibly due to hydroxylation of aluminium oxide (Szetu *et al.*, 2000). Samples A025, A050 and A100 show similar pattern of weight loss event as sample A000 for the first region, second region and fourth region. Nevertheless, the weight loss of samples A025, A050 and A100 in the third region is associated to the template decomposition and the release of water resulting from the phase change to alumina with bimodal porous structure (Aguado *et al.*, 2005). Hence, the adequate calcination temperature for alumina formation and template removal is above 450 °C.
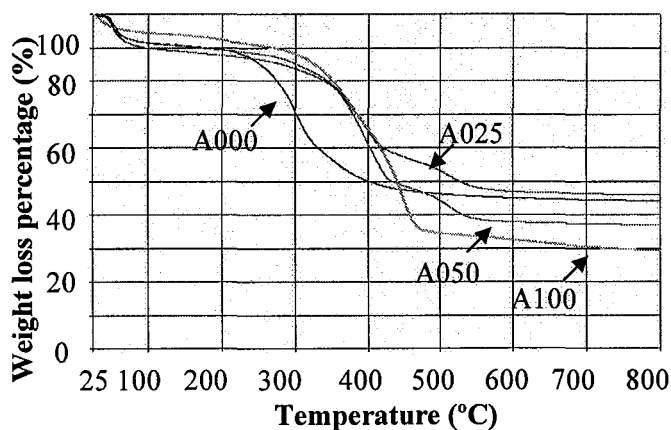

Fig. 3. TGA curves for A000, A025, A050 and A100

Besides sol thermal stability, it is necessary to study the effect of template quantity on sol rheology. This is because sol viscosity is an important factor in sol-gel dip coating operations that affect the films thickness (Jing *et al.*, 2006).The viscosity of the different sols as a function of the rotational speed of the viscometer spindle (which is proportional to the shear rate applied) is shown in Fig. 4. It is found that the sols behave as a Newtonian fluid, exhibiting an almost constant viscosity value within in the whole range of shear rates examined. The Newtonian behavior is exhibited even when the quantity of templating units added is increased. The observed characteristic may be caused by the lack of PS beads agglomerates in the sols (Fu and Tseng, 2006). However, the viscosity of sols increases when more PS beads are added into the sol.
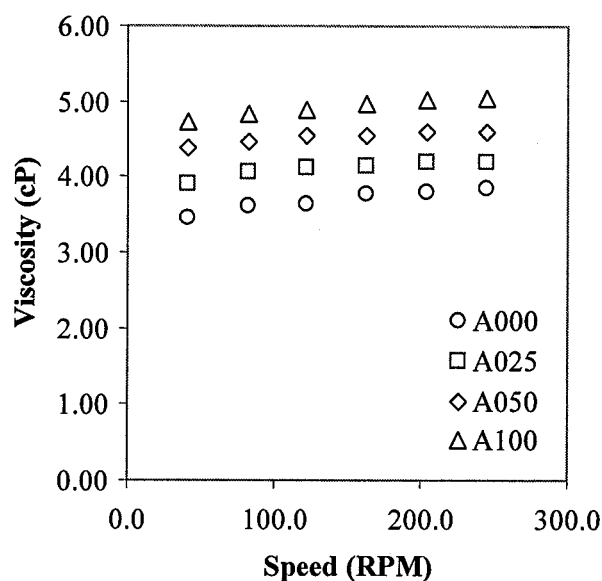
Fig. 4. Viscosity of boehmite sol with different quantity of templating units added.
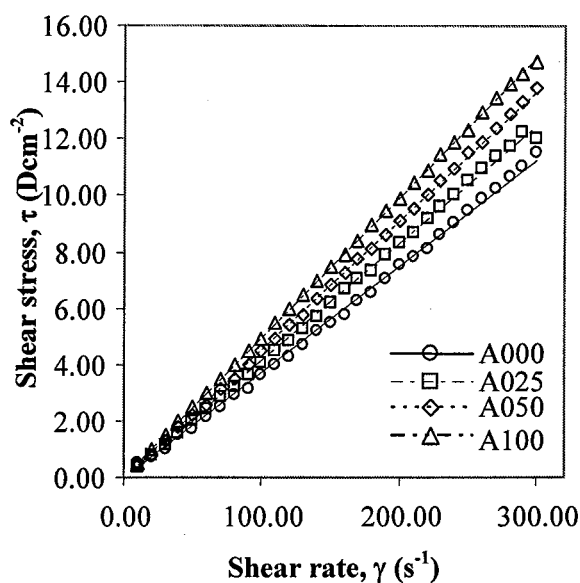
Fig. 5. Newtonian model fit of viscosity for different sols.

The effect of solid template content on the flow behavior of the sols is also presented in Fig. 5. Once again, it is easily observed that the sols show almost Newtonian behavior even the quantity of templating units added increasing. Fitting of observed data to Newtonian model is also shown in Fig.5. with high R^2 (more than 99 %). The viscosity of the sol A000 is 3.74 Pa.s, A025 is 4.15 Pa.s, A050 is 4.56 Pa.s and A100 is 4.94 Pa.s. The viscosity of sol increases when more PS beads are added. It is expected that membrane thickness rises with the increment of secondary pore volume since the viscosity of dip coating sol increases with the increment of template quantity (Jing et al., 2006). Besides that, it should be pointed out that sols also contain 2 wt% of PEG in order to form crack-free thin layers of γ-alumina on top of membrane supports (Lambert and Gonzalez, 1999).

Calcinations at temperature which is higher than 450 °C promotes the removal of PS beads and formation of alumina as explained in the thermogravimetry studies. Hence, all the dried sols are calcined at 500 °C for 1 hr to study the effect of secondary pore volume on γ-alumina characteristics. The microstructure of alumina without secondary pores (A000) can be examined using TEM picture, Fig. 6.
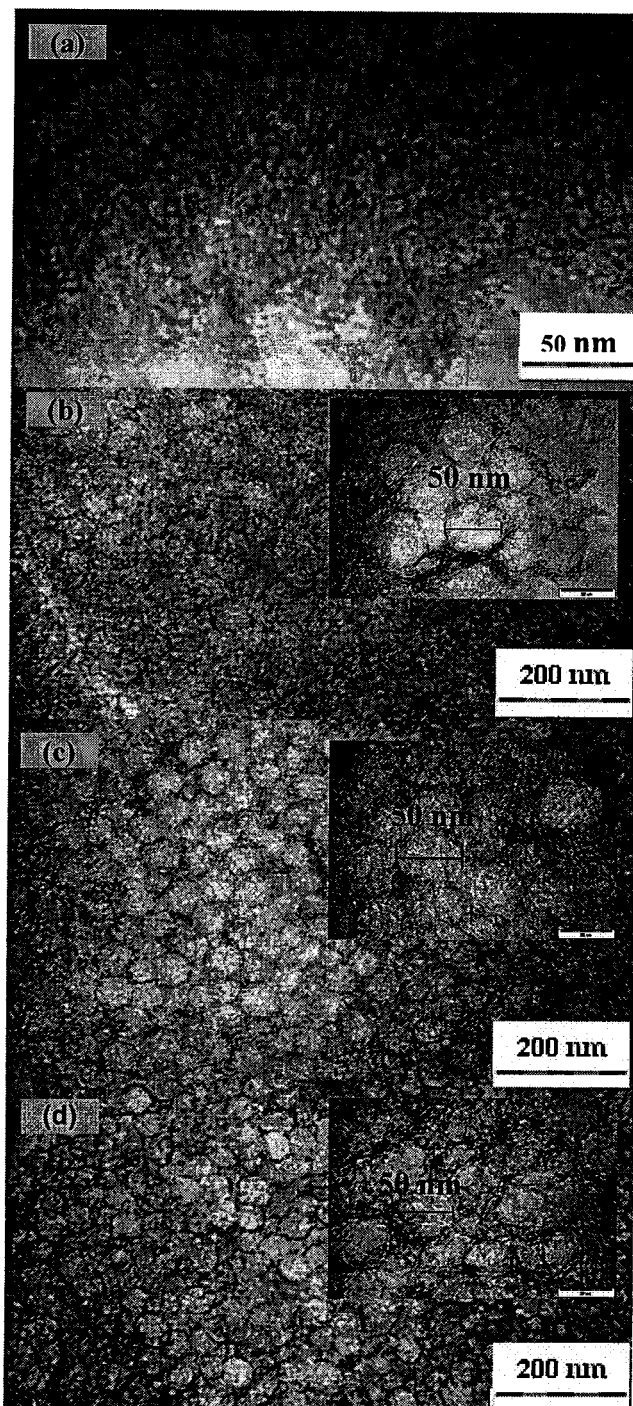

Fig. 6. TEM pictures of (a) A000, (b) A025, (c) A050 and (d) A100 after calcined at 500 °C for 1 hr.

The material is highly porous and the pore diameter is too small to be measured. By adding the nanosized PS beads (diameter ca. 50 nm) into the boehmite sol, additional pores are created in sample A025, A050 and A100 after calcinations at 500 °C for 1 hr. It is generally observed that a well ordered and interconnected porous structure is obtained in sample A025 and A050. The secondary pores can be clearly seen from Fig. 6(b), 6(c) and 6(d). The size of these additional pores is estimated to be close to the size of templating units. Thus, pore shrinkage is not obvious in this work. In addition, pore collapse did not happen even though the samples have been calcined at 500 °C for 1 hr. However, the porous structure of sample A100 is less ordered. It is possibly due to the sol viscosity is too high for proper ordering of spheres using filtration method. During filtration, sphere order can be improved by applying oscillatory shear to the sphere suspension (Vickreva *et al.*, 2000). The method is difficult to be applied in this study since the bimodal porous material has to be coated on top of α-alumina membrane support as thin layer. Oscillatory shear may induce defect on the dip coated thin film. In this study, the amount of PS beads is kept under 0.5 g for each 20 ml boehmite for formation of well ordered secondary pores. There is also no necessacity of creating high secondary pore volume as it might affect the coating of top layer strongly with cracks formed.

FT-IR is an efficient method to measure different types of interatomic bond vibrations at different frequencies. The analysis of IR absorption spectra shows the types of bond which are present in the samples. The FT-IR spectra for all calcined samples are shown in Fig. 7. A000, A025, A050 and A100 are alumina with variation in pore structures. Thus, these four samples show similar FT-IR curves. They show bands at 3404 cm^{-1} to 3467 cm^{-1}, 2072 cm^{-1} to 2088 cm^{-1} and 1636 cm^{-1} to 1644 cm^{-1}. The first band range corresponds to *Al-OH* group (Padmaja *et al.*, 2001). Meanwhile, band at 2072 to 2088 cm^{-1} is possibly due to the presence of water in the samples (Mishra and Rao, 2005). The band range from 1636 cm^{-1} to 1644 cm^{-1} corresponds to the O-H bond bending of adsorbed water and coordinated water (Padmaja *et al.*, 2001). Hence, the samples show the formation of alumina after calcined at 500 °C for 1 hr.
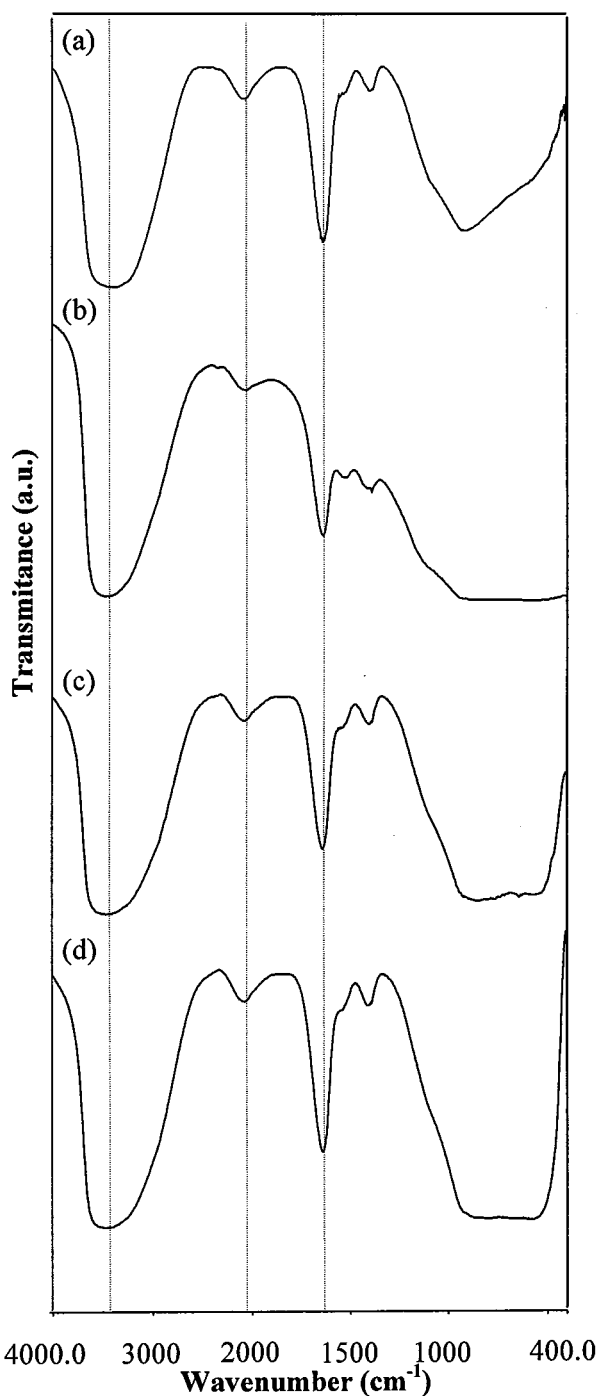
Fig. 7. FT-IR curves of (a) A000, (b) A025, (c) A050 and (d) A100 after calcined at 500 °C for 1 hr.

XRD is used to study the chemical composition and structure of calcined alumina samples with different porous structures. The diffraction angles measured yield the lattice constants, d, pertaining to the crystallographic planes causing diffraction. The XRD patterns of alumina samples with different porous structures are shown in Fig. 8.
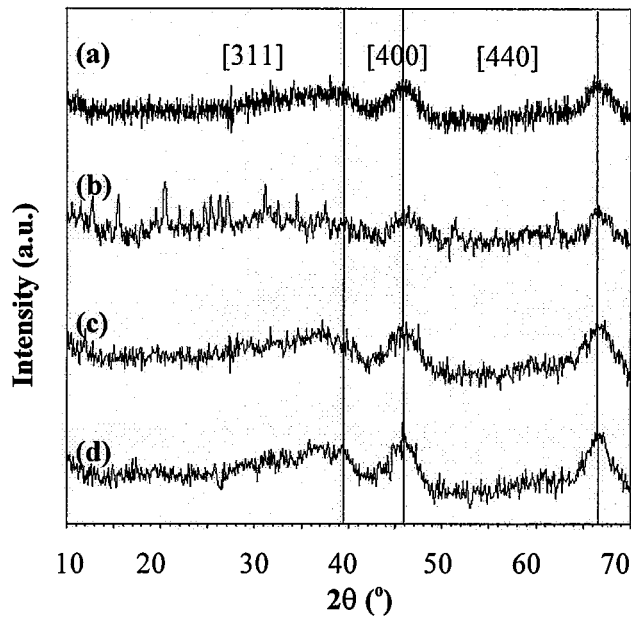
Fig. 8. XRD patterns of (a) A000, (b) A025, (c) A050 and (d) A100 after calcined at 500 °C for 1 hr.

After heat treatment in air at 500 °C for 1 hr, XRD patterns at high angle ($2\theta \sim 10$ - 70 °) are found to be comparatively similar for all the calcined samples of A000, A025, A050 and A100. They show three main peaks placed at d-spacings of 0.242, 0.198 and 0.139 nm respectively, which correspond to the d_{311}, d_{400} and d_{440} reflections of the γ-alumina phase (Aguado et al., 2005). Meanwhile, peaks at $d =$ 6.1, 3.2 and 2.3 Å which correspond to AlO(OH) (JCPDS21-1307) are not found. The result shows that the calcination is adequate to grow crystalline alumina in gamma phase.

Nanosized PS beads shows excellent templating effect in creating secondary pores for sol-gel derived γ-alumina. An ordered and interconnected porous structure can be tailored without serious pore shrinkage or pore collapse. However, ratio of templating units to boehmite sol should be kept at 0.25 g: 20 ml and 0.50 g: 20 ml in order to formed well assembled pores. The increment of secondary pore volume neither affects the chemical composition nor the crystalline structure of γ-alumina.

An understanding of the surface area and porosity of γ-alumina samples can be achieved by the construction of an adsorption/desorption isotherms as shown in Fig. 9. Adsorption isotherms are obtained point-by-point by admitting to the adsorbent successive known volumes of nitrogen and measuring the equilibrium pressure. Similarly, desorption isotherms are acquired by measuring the quantities of gas removed from the sample as the relative pressure is lowered. All samples show isotherms of type IV in the Brunauer, Deming, Deming and Teller classification (Gregg and Sing, 1991). The isotherms are associated with capillary condensation in mesopores, indicated by the steep slope at higher relative pressure. Isotherms of sample A000, A025 and A050 also show hysteresis loop at a relative pressure of approximately 0.6. The type E hysteresis loops according the original de Boer classification (de Boer, 1958) appear in the isotherms.
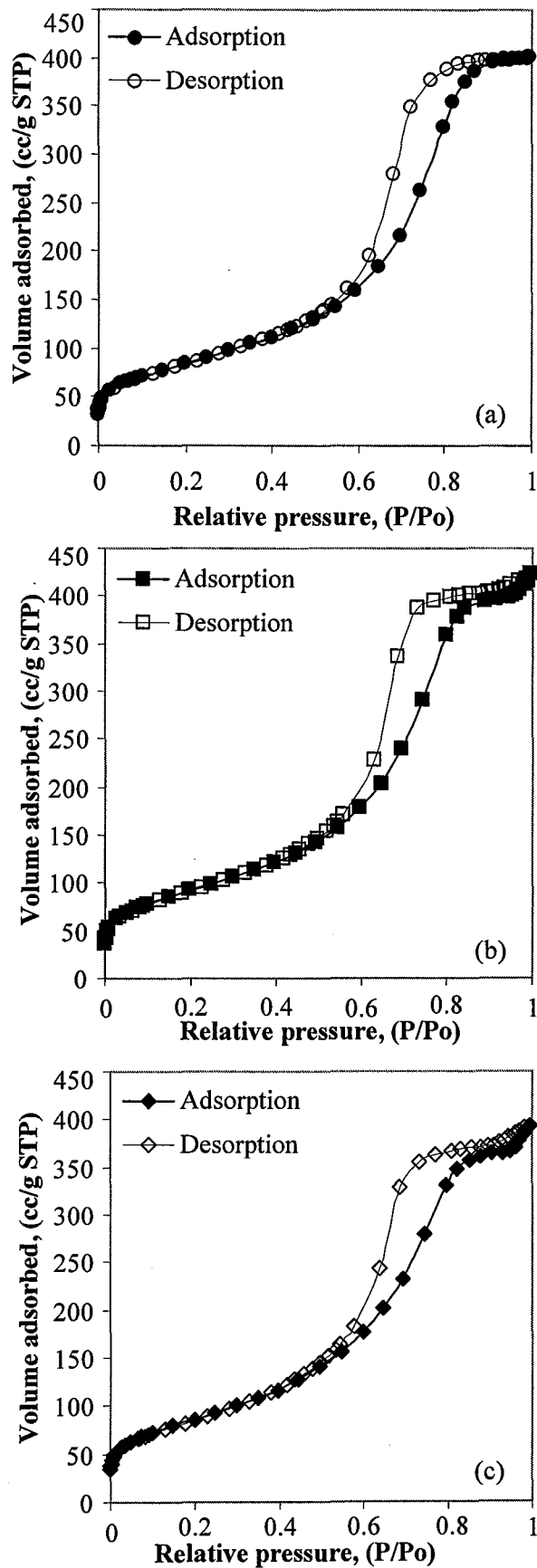
Fig. 9. N_2 adsorption and desorption isotherms for (a) A000, (b) A025 and (c) A050 after calcined at 500 °C for 1 hr.

This type of hysteresis loops indicate the presence of "ink-bottle" type pores in the mesoporous γ-alumina samples (Sangwichien *et al.*, 2002). The hysteresis loops in the isotherms close before reaching a relative pressure of 0.3 in the desorption process as there is no micropores.

The distributions of pore volume with respect to pore size for γ-alumina with different porous structures are shown in Fig. 10. It is generally accepted that the desorption isotherms is more appropriate than the adsorption isotherm for evaluating the pore size distribution of an adsorbent. This is because the desorption branch of the isotherm, for the same volume of gas, exhibits a lower relative pressure, resulting in a low free energy state (Micromeritics®, 1992). Thus, the desorption isotherms are closer to true thermodynamic stability.

Fig. 10. Pore size distribution of γ-alumina samples based on the BJH-model for the desorption branch of the nitrogen isotherms.

The pore size distribution of γ-alumina samples for the desorption branch is calculated using Barrett-Joiner-Halenda (BJH) method. From Fig. 10, sample A000 shows narrow pore size distribution with average pore diameter of 5.76 nm which is close to pore size reported by Lambert et al. (1999). As the same boehmite sol is used for the preparation of sample A025 and A050, both samples show primary pore diameter which is close to sample A000. Meanwhile, 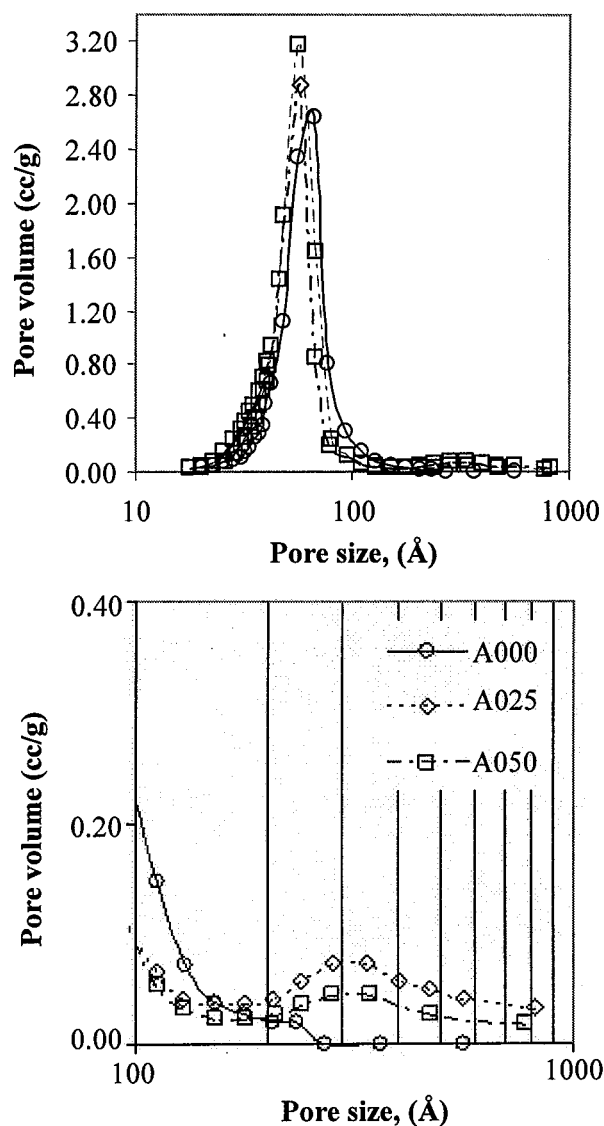secondary pore size distribution is observed in Fig. 10 for sample A025 and A050. The secondary pore volume in sample A050 is higher than sample A025 as more templating units have been added into A050 sol. However, BJH method is not suitable for estimation of secondary pore size. In Fig. 10, the mean secondary pore size is estimated at 30 nm which is far from secondary pore size which is measured using TEM. This is possibly because N_2 adsorption/desorption method is generally not very accurate in membrane with a large pore size distribution and without a definite pore geometry (Mulder, 1996). The measured BET surface area, total pore volume and average pore diameter of samples A000, A025 and A050 are summarized in Table 1.

Table 1 Characteristic of the mesoporous γ-alumina samples after calcined at 500 °C for 1 hr

Sample	BET surface area (m^2/g)	Total pore volume (cm^3/g)	Average pore diameter (nm)
A000	301.1	0.61	5.7
A025	310.2	0.60	5.2
A050	330.2	0.64	5.5

3.2 Bi-layered Membrane with Bimodal Porous Intermediate Layer: Improved Permeability

Bimodal porous ceramics are usually utilized as catalyst supports with reduced transport resistance for reactants to reach the active sites rapidly (Takahashi et al., 2001). Unlike the conventional approach, bimodal porous γ-alumina is employed as a membrane in this study. The γ-alumina with bimodal pore size distribution which has been optimized in the previous section is tailored into thin films using dip-coating method. Surfactant templated silica is later dip-coated on top of the γ-alumina layer in order to form a bi-layered membrane. Characteristics of membranes such as permeability, pore size, and ratio of membrane thickness to porosity are determined using the water permeability test and the PEG retention test.

Supported γ-alumina thin layers can be scrutinized using SEM technique. Thin layers of γ-alumina with different porous structures are successfully formed after calcinations of A000, A025 and A050 coatings on alumina supports (Fig. 11). There is no formation of serious defects such as cracks or pin holes. The final thickness of γ-alumina membranes with different porous structures can be also determined from membrane cross-sectional micrographs (Fig. 11). Although dip-coated liquid film thickness can be predicted from Landau–Levich–Derjaguin (LLD) equation (Equation 1), there is uncertainty of LLD equation due to thickness change after film hardening and oxidation (Jing et al., 2006).
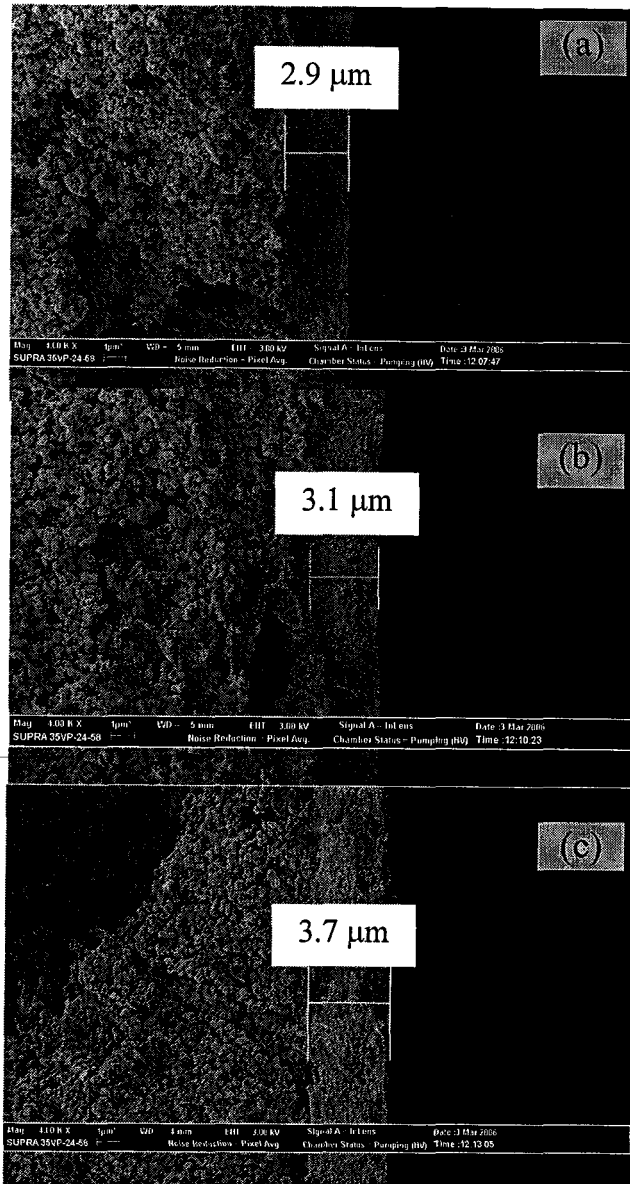
Fig. 19. SEM pictures of (a) A000, (b) A025 and (c) A050 supported on α-alumina discs.

$$H = 0.94 \frac{(\eta \cdot U)^{2/3}}{\gamma LV^{1/6} \cdot (\rho \cdot g)^{1/2}} \tag{1}$$

where H is the liquid film thickness, U is the withdrawal speed, η is the viscosity, ρ is the density, γLV is the liquid–vapor surface tension and g is the acceleration due to gravity (Jing *et al.*, 2006). It only predicts liquid film thickness in sol-gel dip coating operations before drying and calcinations. Thus, SEM is the most reliable method to measure the membrane thickness after hardening and oxidation in calcination step. The thickness of γ-alumina thin layers is ca. 3 − 4 μm after single dip-coating and calcinations. The γ-alumina membrane thickness in this work is close to membrane thickness reported by Ulhorn *et al.* (1992) and Chowdhury *et al.* (2006). The reported membrane thickness is 3 − 5 μm where boehmite sol is also employed in their study. However, it is observed that the thickness of the

21

thin layers increases from A000 to A050. It is likely due to the increment of sol viscosity as previously measured. The increment of sol viscosity raises the dip-coated liquid film thickness as shown in LLD equation (Equation 1). Consequently, the thickness of membranes grows from A000 to A050 even after hardening, oxidation and removal of template.

Membranes are always rated for their permeate flux and rejection level. Flux is the term used to describe how fast a product passes through a membrane. Referring to Darcy's law, the liquid flux is proportional to the applied pressure when transport mechanism obeys the viscous flow model. The membrane permeability is defined as the permeation coefficient in this law and it represents the economical level of a membrane. The operational cost of membrane separation can be reduced by using membranes with higher permeability.

The pure water permeative behavior of γ-alumina membranes with different porous structures are shown in Fig. 12. A000 membrane shows the lowest permeability among the γ-alumina membranes.
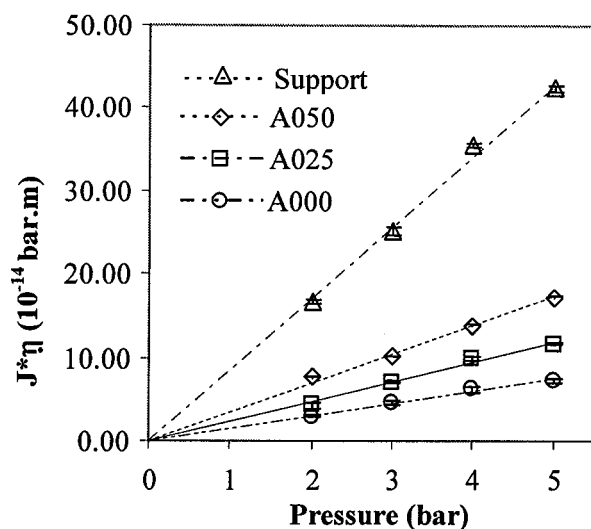
Fig. 12. Product of water flux and viscosity vs. applied pressure of γ-alumina thin layers with different porous structures supported on α-alumina support.

The conventional γ-alumina membrane (A000) achieves poorer permeate flux at pressure 1 - 5 bar compared to γ-alumina membranes with secondary pores (A025 and A050). When the secondary pore volume increases, it is also observed that the water permeability of γ-alumina membranes improves. The overall membrane permeability coefficients (k_m) are calculated using Darcy's Law and summarized in Table 2. The overall membrane permeability coefficients (k_m) can be also deconvoluted into the permeability coefficients of the α-alumina support and the γ-alumina thin layer respectively. From Table 2, the permeability coefficient of γ-alumina thin layer increases 79.17 % when a moderate secondary pore volume is created in A025. The permeability coefficient achieves even more than 200 % increment when a high secondary pore volume is tailored in A050.

Specific resistance of membrane is another important parameter that eliminates the effect of membrane thickness in calculating the resistance of membranes to the permeation. The specific resistance r_m of membranes to the permeation is summarized in Table 2.

Table 2 Calculated permeability coefficients k_γ and specific resistance r_m for γ-alumina thin layers with different porosity

Coating	Support	Overall Permeability, $k_m (10^{-14}\,m)$	Thin Layer Permeabilty $k_\gamma (10^{-14}\,m)$	Specific Resistance $r_m (10^{19}\,m^{-2})$
A000	α-alumina	1.50	1.82	1.90
A025	α-alumina	2.36	3.26	0.99
A050	α-alumina	3.47	5.82	0.46
None	α-alumina	8.57	N/A	N/A

The conventional γ-alumina thin layer (A000) in this work shows specific resistance of $1.90 \times 10^{19}\,m^{-2}$ which is smaller than the specific resistance reported by De Lint and Benes ($3.45 - 6.25 \times 10^{19}\,m^{-2}$) (2005). The difference of specific resistance is possibly because A000 possesses much larger pores compared to γ-alumina in their work (pore diameter ≈ 2 nm). The average pore diameter of unsupported γ-alumina A000 is measured at 5.7 nm as shown in Table 1. Meanwhile, Chowdhury et al. (2006) reported only slightly higher specific resistance of γ-alumina membrane ($2.0 \times 10^{19}\,m^{-2}$) compared to A000. The average pore diameter reported by Chowdhury et al. (2006), however, is much bigger (8.6 nm). Thus, the great specific resistance of γ-alumina membrane in their work is possibly due to low membrane porosity. From Table 2, it is obvious that the creation of secondary pores in γ-alumina further enhances the diminution of transport resistance. The specific resistance of γ-alumina membrane decreases almost 48 % to 76 % when secondary pores are templated at different pore volumes.

For comparing the performance of membranes, it is also necessary to understand their rejection characteristics through permeation process. Quantification of rejection properties is very important when comparing performance of membranes with small pores such as NF, since small deviations in pore size can be translated into different rejection capabilities with significant differences for solutes of interest (Cleveland et al., 2002). Most manufacturers of NF membranes rate their pore size with a molecular weight cutoff (MWCO). Most often MWCO is described as the upper molecular weight limit of transport which is equivalent to a 90 % rejection (Cooper and Van Derveer, 1979). The rejection characteristics can be determined using solutes that are more or less retained by the membrane ('cut-off' measurement). From Fig. 13, the γ-alumina thin layer without secondary pores (A000) shows more than 90 % retention for PEG with molecular weight higher than 10500 Da. The MWCO of γ-alumina membrane in this work is slightly higher compared to other works. The MWCO

of γ-alumina membrane are approximately in the range of 2000 to 10000 with PVA added in the sol as reported by Uhlhorn *et al.* (1992), Peterson *et al.* (1990), Burggraaf *et al.* (1989, 1991) and Leenars *et al.* (1984, 1985). In general, MWCO of γ-alumina membrane increases with the calcination temperature as particle grew in size. A further increment of calcination temperature (above 1000 °C) not only involved a phase transition of γ-alumina to α-alumina, but also resulted in the conversion of the UF membranes to MF membranes. As calcination temperature in this work is only 500 °C, it is not the main factor that causes the high MWCO of γ-alumina membrane.
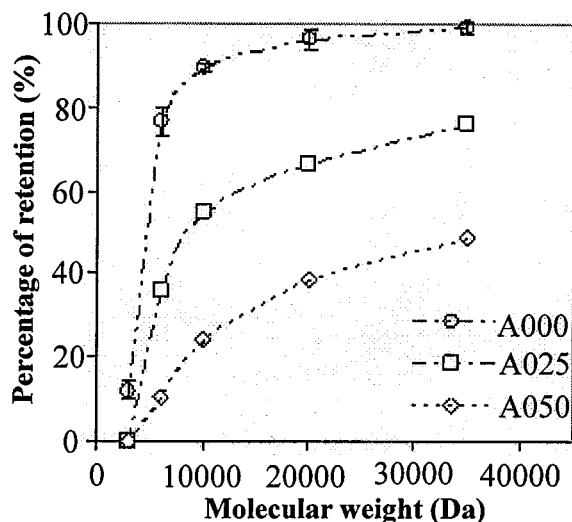
Fig. 13. PEG retention curves of different γ-alumina thin layers at 4 bar.

According to Lambert and Gonzalez (1999), the addition of PEG can cause a growth of membrane pore volume and pore diameter compared to membranes prepared with PVA added as binder. Thus, the addition of PEG into the boehmite sol may cause a higher MWCO of γ-alumina membrane in this work. Besides that, the preparation methodology is another possible factor that causes the difference in membrane MWCO. For example, γ-alumina membranes with extreme low MWCO (350 - 450 Da) can be prepared using a "flash" firing treatment (Larbot *et al.*, 1994). In order to make conclusions about pore size, the molecular weight of PEG is correlated to its Stokes–Einstein radius. The average pore size of conventional γ-alumina membrane (A000) is estimated at 5.3 nm. The estimation is close to pore size of unsupported A000 which is measured using N_2 adsorption/desorption in Section B.1.

For A025 and A050 membranes, the retention is lower than 90 % even for PEG 35000 with the creation of secondary mesopores (50 nm). This is reasonable as the secondary pore radius (ca. 25 nm) is much bigger than stokes radius of PEG 35000 (4.87 nm). Unlike conventional membranes with unimodal pore size distribution; there is still some retention of PEG molecules (6000 – 35000 Da) through bimodal porous membranes as shown in Fig. 13. A025 and A050 do not show extremely high permeation of PEG molecules which are much smaller compared to its secondary pores. This may due

to tremendously low secondary pore volume in A025 and A050 compared to primary pore volume as shown in Fig. 10.

Besides explaining membrane permeability using phenomenal model, transport through porous membrane can be related to its porous structure. The simplest model is Hagen-Poiseuille where membrane porous structure is considered as a number of parallel cylindrical pores. However, the solvent flux through bimodal porous membrane is due to the permeation of solvent through primary pores and secondary pores. Bimodal porous membrane are considered possessing two types of cylindrical pores with different corresponding porosity as stated in Equation 2.

$$ k_m = \frac{r_{p1}^2}{8(\Delta x_1 / A_{k1})} + \frac{r_{p2}^2}{8(\Delta x_2 / A_{k2})} \tag{2} $$

The secondary porosity in A025 and A050 samples is calculated by assuming the length of all cylindrical pores is almost equal to the membrane thickness and the primary porous structure of the bimodal porous membranes is identical to the porous structure of unimodal porous membrane (A000). The results of porosity calculation are shown in Table 3.

Table 3 Secondary porosity in bimodal porous γ-alumina

Membrane	k_m $(10^{-14}, m)$	k_2 $(10^{-14}, m)$	r_{p1} (nm)	r_{p2} (nm)	L (μm)	A_{k1}	A_{k2}
A000	1.82	0	5.3	0	2.9	0.06	0
A025	3.26	1.31	5.3	50	3.1	0.06	0.0005
A050	5.82	3.50	5.3	50	3.7	0.06	0.0016

From the calculation, it is obvious that secondary porosity is extremely low compared to primary porosity. The calculation is parallel with the pore volume measurement using N_2 adsorption/desorption (Fig. 10). However, the secondary pores are able to enhance the permeability of γ-alumina membrane greatly as the secondary pore size is ca. 10 times of the primary pore size. Although amount of templating units added in A050 is 2 times of amount of templating units added in A025, the secondary porosity of A050 is higher than the expected value. This is possibly because that the configuration of the pores (cylindrical) used in the Hagen-Poiseuille model description deviate dramatically from the actual morphology (Mulder, 1996).

In this work, ordered porous silica has been tailored using micellar solution of CTAB which transforms to a hexagonal phase in the presence of silicate anions. Common characterization methods such as TEM, XRD and N_2 adsorption/desorption are used to confirm the formation of ordered pores. Fig. 14 shows the TEM micrograph of surfactant templated silica (designated as Si) after calcined at 450 °C for 1.5 hr. A superstructure is clearly visible in Si. It has a periodicity of about 4 nm, and found to be oriented in a certain direction. Fig. 15 shows the XRD pattern for surfactant templated silica with

ordered mesopores. It shows the existence of a broad peak at 2.5 °, indicating the presence of long range order (Boffa et al., 2007).
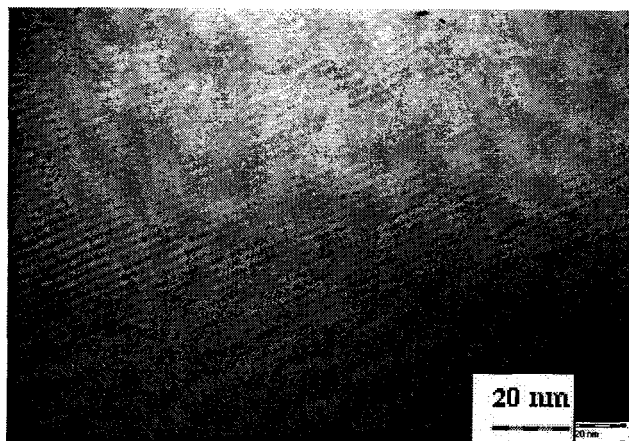
Fig. 14. TEM pictures of Si.
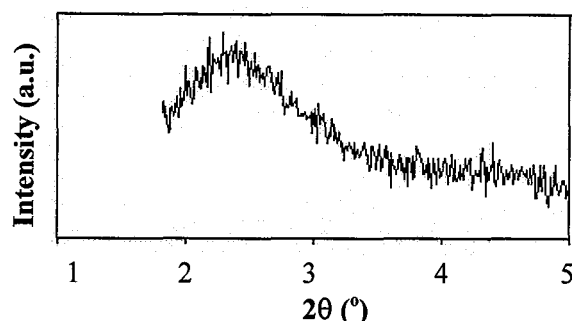
Fig. 15. XRD pattern of Si with ordered nanopores after calcinations.

The N_2 adsorption isotherms over the entire relative pressure range of the surfactant templated silica are shown in Fig. 16. As expected, the adsorption isotherm is of type I (according to Brunner, Deming, Deming and Teller classification) or Langmuir type which indicates that the surfactant templated silica is microporous solid. The limiting uptake of adsorbate is governed by the accessible micropore volume rather than by the internal surface area. The BET surface area (975.3 m^2/g) and the total pore volume (0.56 cm^3/g) of surfactant templated silica are satisfactory. The porous material shows reasonable surface area and pore volume compared to other types of surfactant templated silica such as MCM-41 material which possesses a surface area in the range of 950 - 1120 m^2/g and a pore volume in the range of 0.66 - 1.78 cm^3/g (Choma and Jaroniec, 2007). When evaluating the pore size distribution from nitrogen isotherm data, methods that employ the Kelvin equation, especially the BJH method, are generally used (Fig. 17). However, it is found that BJH method is not a good way for calculating micropore size as micropore volume is undetermined in this sample (Jaroniec and Solovyov, 2006).
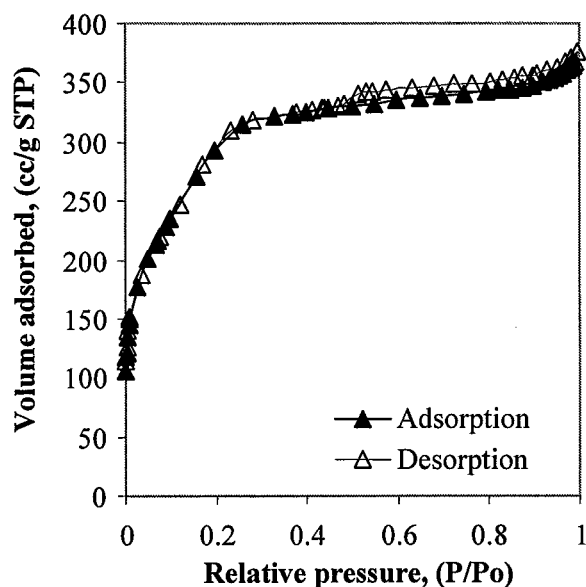
Fig. 16. N_2 adsorption and desorption isotherms for silica after calcined at 450 °C for 45 min.
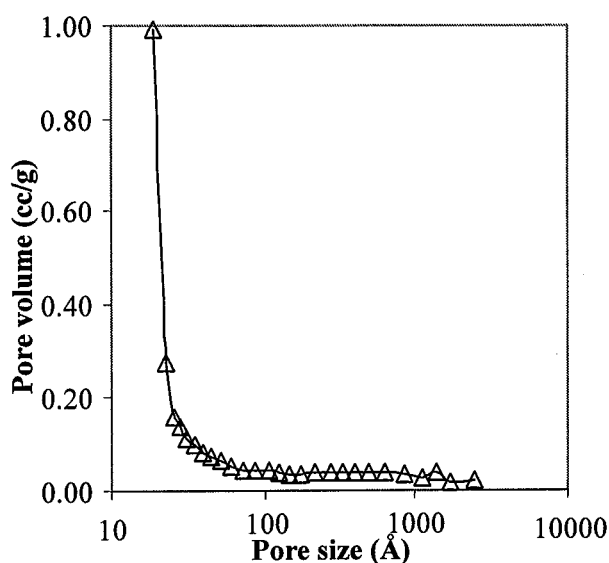
Fig. 17. Pore size distribution of silica sample based on the BJH model for the desorption branch of the nitrogen isotherms.

For better micropore analysis, t-method is used for the estimation of micropore size. The observation of two linear regions in the t-plot (Fig. 18) indicates the presence of micropores which is larger than 7 Å. The actual pore width ($2t$) can be estimated at the position where two linear plots intersect as it signifies that the filling of micropores is taking place (Aguilar-Armenta and Díaz-Jiménez, 2001). Thus, the average pore size of the surfactant templated silica is estimated about 10 Å. The estimated pore size is smaller than the pore size reported by Chowdhury et al. (2006) where the average pore size of the similar silica supported on γ-alumina is estimated to be approximately 18 Å.
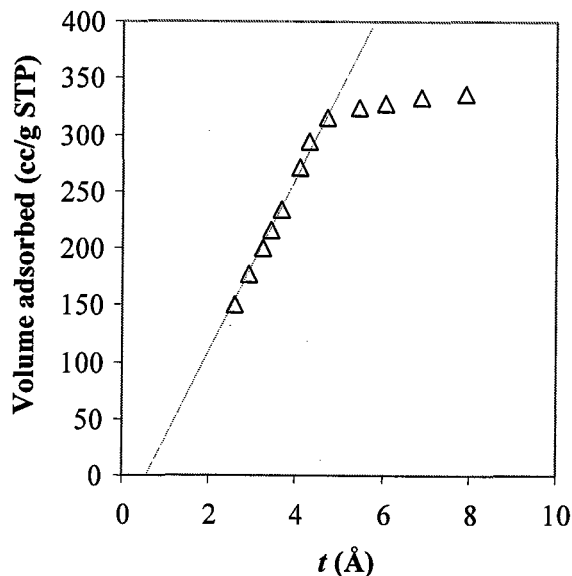
Fig. 18. The *t*-plot of surfactant templated silica after calcined at 450 °C for 45 min.

Ordered pores have been successfully tailored in silica using the synthesis method introduced by Honma *et al.* (2000). The average pore size (10 Å) and the BET surface area (975.3 m^2/g) of unsupported silica are reasonable compared to literatures. The silica is then coated on γ-alumina thin layers with different porous structures (A000, A025 and A050) for preparing silica/ γ-alumina membranes.

In the current section, characteristics of silica/γ-alumina membranes with different intermediate layers are studied. The surfactant templated silica is coated on γ-alumina layers with different secondary pore volumes (A000, A025 and A050). It is interesting to study the effect of secondary pores (ca. 50 nm) on the formation of silica thin layers. This is because the existence of secondary pores in the intermediate layer may cause different levels of silica sol infiltration. It is possible that silica layers form at different coordinates in the membrane. The variation of membrane structures may lead to changes of membrane performance. In this study, the membrane performance is rated using water permeability test and PEG retention test. The effect of secondary pore volume on the overall membrane performance is investigated and discussed in this section.

Silica/γ-alumina membranes with different porous structures in intermediate layers can be scrutinized using Fig. 19. Although the γ-alumina membranes (A000, A025 and A050) have been dip-coated with silica sol twice, no formation of silica layer on top can be found after calcinations. Filtration of silica sol into the subsequent layer obviously happened. From EDX analyses of silica distribution, it is observed that the silica has been deposited in the pores of γ-alumina layers (Fig. 19(d), 19(e) and 19(f)). However, the density of silica layers reduces from membrane A000/Si to A050/Si. The reduction of silica density may be caused by the increment of secondary pores in the intermediate layers. It is also observed that the silica layers are well formed on top of α-alumina supports in A00/Si and A025/Si membranes. However, silica layer is not so well formed in A050/Si

28

membrane. This is likely because bimodal porous structure of A050 is inadequate to prevent penetration of silica sol into α-alumina support during dip-coating.
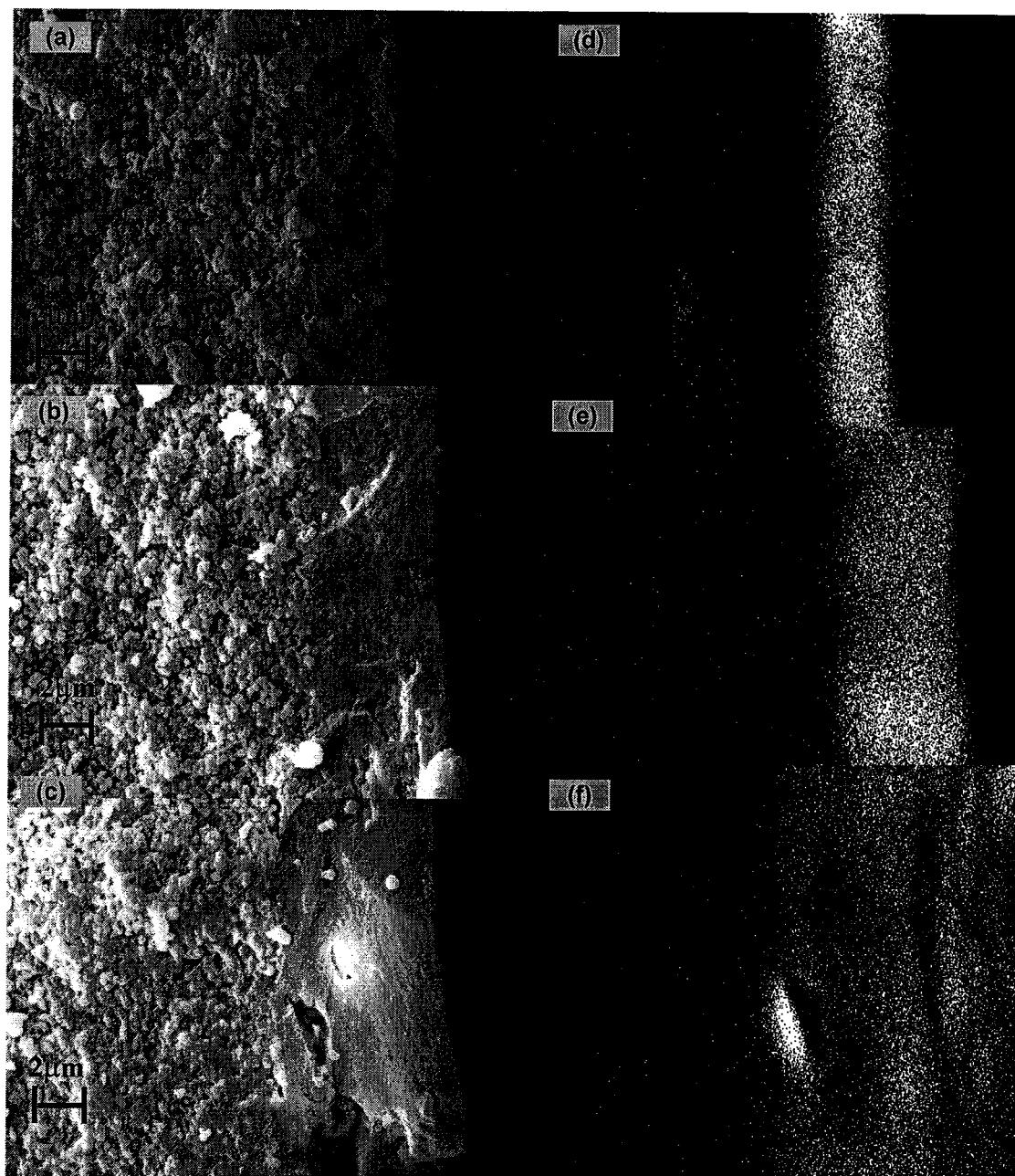
Fig. 19. SEM and EDX images of the bi-layered membrane prepared with different intermediate layers (a) SEM image of A000/Si membrane, (b) SEM image of A025/Si membrane, (c) SEM image of A050/Si membrane, (d) the distribution of Si on A000/Si membrane by EDX (e) the distribution of Si on A025/Si membrane by EDX and (f) the distribution of Si on A050/Si membrane by EDX.

The plot of steady state water flux versus pressure for silica membranes supported γ-alumina with different secondary pore volumes (A000, A025 and A050) is illustrated in Fig. 20. The water flux

is proportional to the applied pressure obeying Darcy's law. Apparently, the permeate flux through bi-layered membranes increases with the rising of secondary pore volume in the intermediate layer.
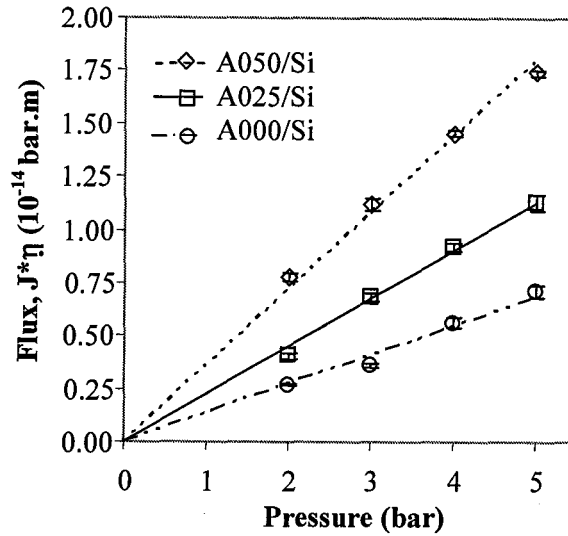
Fig. 20. Product of water flux and viscosity vs. applied pressure of bi-layered membranes with different intermediate layers supported on α-alumina support.

Using Darcy's law, the overall liquid permeability of bi-layered membranes is calculated. The summary of the calculations is shown in Table 4. The overall liquid permeability of bi-layered membranes increases when more secondary pores are introduced into the intermediate layer. The overall liquid permeability of bi-layered membranes raises almost 64 % when γ-alumina with relative low secondary pore volume (A025) is employed as the intermediate layer. For a bi-layered membrane consisting γ-alumina with high secondary pore volume (A050), the increment of overall liquid permeability is more than 162 %.

Table 4 Overall permeability and thickness for silica/γ-alumina membranes

Sample	Top layer	Intermediate layer	Support	Overall permeability, k_m (10^{-14} m)	L_γ (μm)	L_{Si} (μm)
A000/Si	Silica	A000	α-alumina	0.14	3.3	3.0
A025/Si	Silica	A025	α-alumina	0.23	4.8	4.7
A050/Si	Silica	A050	α-alumina	0.36	5.7	5.6

Of course, it is inquisitive to find out the contribution of each layer in the bi-layered membranes to the permeability improvement. The permeability of individual layer in the bi-layered membranes is determined using Darcy's law and information in Table 2. The results of calculation are

summarized in Table 5. From Table 5, it is observed that the creation of secondary pores in the intermediate layer affects the separation characteristic of supported silica layer. The specific resistance of silica layers reduces 62 – 80 % when coated on bimodal porous γ-alumina layer. The results are rational as the silica density reduces with increment of secondary pore volume in γ-alumina layer as shown in EDX analyses (Fig. 18).

Table 5 Permeability and specific resistance of silica layers supported with different intermediate layers (A000, A025 and A050)

Sample	Permeability for γ-alumina layer, k_γ (10^{-14} m)	Permeability for silica layer, k_{Si} (10^{-14} m)	Specific resistance for silica layer, R_{Si} (10^{19} m^{-2})
A000/Si	1.60	0.15	22.18
A025/Si	2.10	0.25	8.43
A050/Si	3.78	0.40	4.48

The improved membranes, A050/Si shows more than 90 % retention of PEG 600 while A025/Si shows more than 90 % retention of PEG 400 at 400 kPa (Fig. 21). The MWCO of A025/Si membrane is observed to be close to the MWCO of conventional bi-layered membrane (A000/Si). The average pore radius of silica layers can be determined based on their MWCO using Equation 3.

$$r = 0.262 \times (MW)^{1/2} - 0.3 \tag{3}$$

where r is molecular radius (Å) and MW is molecular weight (Da).The average pore radius of silica layer in A000/Si and A025/Si is 0.5 nm while the average pore radius of silica layer in A050/Si membrane is 0.6 nm. Coating silica on γ-alumina with similar primary pore size (5 - 6 nm) but dissimilar secondary pore volume seems to form slightly different pore size in silica. Chowdhury et al. (2006) reported that the pore radius of surfactant silica is much bigger (1.0 nm) when coated on γ-alumina with average pore diameter of 8.6 nm. Obviously, porous structures of intermediate layers show a significant effect on the pore size of top layers. Specifically, the porosity of silica layer is affected by the occurrence of secondary pores in γ-alumina layer. The reduction of silica density as observed in the EDX analyses can be related to the increment of silica porosity as calculated using Equation 4.

$$k_m = \frac{r_p^{2}}{8(\Delta x / A_k)} \tag{4}$$

Table 5.14 shows the calculated pore size (r_p), the ratio of effective membrane thickness to membrane porosity ($\Delta x/A_k$) and the porosity of silica layers (A_k) coated on γ-alumina layers with different secondary pore volume.
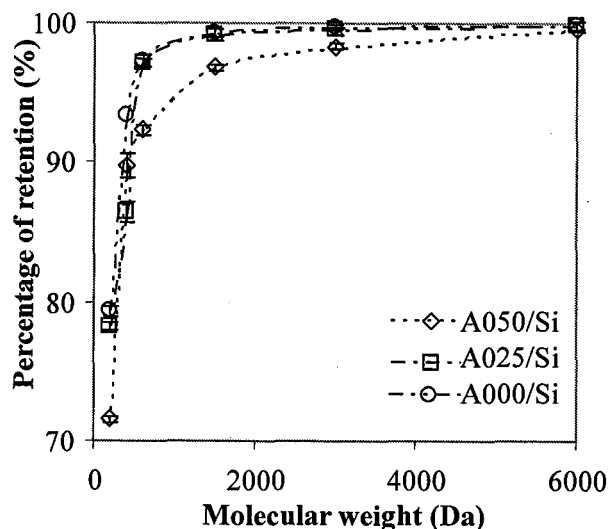
Fig. 21. PEG retention curves of different membranes at 4 bar.

Table 6 Pore size and porosity of silica layers supported with different intermediate layers (A000, A025 and A050)

Sample	r_p (nm)	$\Delta x/A_k$ (10^{-5}m)	A_k
A000/Si	0.5	2.08	0.14
A025/Si	0.5	1.24	0.38
A050/Si	0.6	1.13	0.49

A025 thin layer appears to be the most appropriate surface for the formation of a silica membrane with improved permeability and reserved retention. This is because A025 is able to prevent penetration of silica sol into α-alumina support. The silica layer is formed on top of the membrane support with low silica density. Consequently, the permeability of silica layer is improved. In addition, the bimodal porous A025 layer also introduces a lower transport resistance to bi-layered membrane compared with unimodal porous A000.

An improvement in membrane permeability always brings a trade off in membrane MWCO unless pore enlargement is not involved. This can be done by reducing the membrane thickness and/or improving the membrane porosity. The membrane porosity includes the surface porosity and the pore tortuosity. In this study, the permeability enhancement of silica/γ-alumina membrane is possibly due to the improvement of membrane porosity which involves a density reduction of separating layer and secondary pore creation of intermediate layer.

3.3 Dye and Salt Transport Characteristics of Bi-layered Membranes with Different Secondary Pore Volumes

Besides providing an appropriate medium for the formation of silica layer, γ-alumina layer contributes to ions retention at pH near to the IEP of silica layer as reported by Samuel de Lint *et al.* (2006). In addition to the improved ion separation performance, this may also be a fast and effective way to reduce the exposure of the penetrated separating layer to harsh pH conditions. Due to retention, the exposed layer can reduce the concentration of strong acid or base within the penetrated layer or alternatively to prevent fouling of the membrane. This section is intended to study the ion separation performance of silica/γ-alumina membranes with different secondary pore volumes. The study includes the investigation of operating variables effect on large organic ions (dyes) separation and small inorganic ions (salt) separation from aqueous solution when membranes with different secondary pore volume (A000/Si, A025/Si and A050/Si) are employed. For *NaCl* separation, ENP Model is used to characterize the separation characteristics of bi-layered membrane with different porous structures.

Reactive dyes are water soluble so they cannot be easily removed using physical methods such as coagulation or adsorption. Compared to advanced chemical oxidation and adsorption, NF is the most economical method to eliminate reactive dyes in wastewater. Thus, the main objective of this section is to investigate the dye separation performance of bi-layered membranes with different secondary pore volumes. Three types of reactive dye with variation in molecular weight are used in this study. The characteristics of these reactive dyes such as their molecular weight, number of charge, structure and the compact formula (Sigma-Aldrich, 2007) are listed in Table 7.

Table 7 Characteristics of the reactive dyes used

Dye	Molecular weight, (Da)	Charge	Structure
RR120	1469.98	-6	

Table 7 Continued

Dye	Molecular weight, (Da)	Charge	Structure
RB5	991.82	-3	
RO16	617.54	-1	

The variation of dye rejection at pressure in the range of 4 – 10 bar for A000/Si, A025/Si and A050/Si membranes is shown in Fig. 22. In general, the rejection of RR120 is highest and followed by RB5 and RO16. This is because the sieving mechanism reduces when the molecular weight of dyes approaches the MWCO of membrane (400 – 600 Da). The non-spherical organic ions may escape from the membrane pores at certain orientation (Santos *et al.*, 2006). Besides that, electrostatic interactions between charged solutes and a porous membrane have been frequently reported to be an important mechanism (Bellona *et al.*, 2004). The lower charge numbers of RB5 and RO 16 compared to RR120 may cause the diminution of repulsion force at the membrane surface and lead to lower rejection. The rejection of RR120 is most satisfactory as 95 % of the dye can be removed using A000/Si, A025/Si and A050/Si membranes regardless of the pressure changes. There is a high possibility that the separation is mainly influenced by sieving mechanism since the molecular weight of RR120 is much bigger than the MWCO of A000/Si, A025/Si and A050/Si membranes (400 – 600 Da) (Akbari *et al.*, 2002). For smaller dye, the rejection of RB5 and RO16 decreases with the increment of pressure. The observation is most possibly due to the growth of membrane surface concentration. The rising pressure promotes the convective flux and leads to the enhancement of the

concentration polarization (Mulder, 1996). When the surfactant templated silica is coated on γ-alumina with unimodal pore distribution (A000/Si), it is observed that RB5 dye and RO16 dye are well rejected (Fig. 22(a)).

Fig. 21. Retention of RR120, RB5 and RO16 dyes solution with concentration of 1000ppm at different pressure using (a) A000/Si (b) A025/Si and (c) A050/Si membranes.

All the dye retention achieves more than 80 % for trans-membrane pressure varied from 4 bar to 10 bar. By coating on top of γ-alumina with low secondary pore volume (A025), the silica membrane rejects nearly 80 % RO16 dye from water even at a pressure as high as 10 bar. This shows likelihood

that defects such as cracks and pinholes is absent in the silica layer formed in A025/Si membrane as it is able to reject organic ions with molecular weight smaller than 1000 Da. It is proven again that γ-alumina with low secondary pore volume (A025) has successfully facilitated the formation of silica layer with sufficient density. Nevertheless, membrane A050/Si only rejects RB5 at acceptable retention percentage, more than 80 %. The retention of RO16 which is smaller in size only reaches 44 % at the lowest pressure. This is possibly because the silica layer of membrane A050/Si is less dense and unable to provide enough repulsion force for the rejection of small charged solute.

The rejection of dyes in feed solutions with different concentrations at 10 bar using (a) A000/Si (b) A025/Si and (c) A050/Si membrane is shown in Fig. 23.
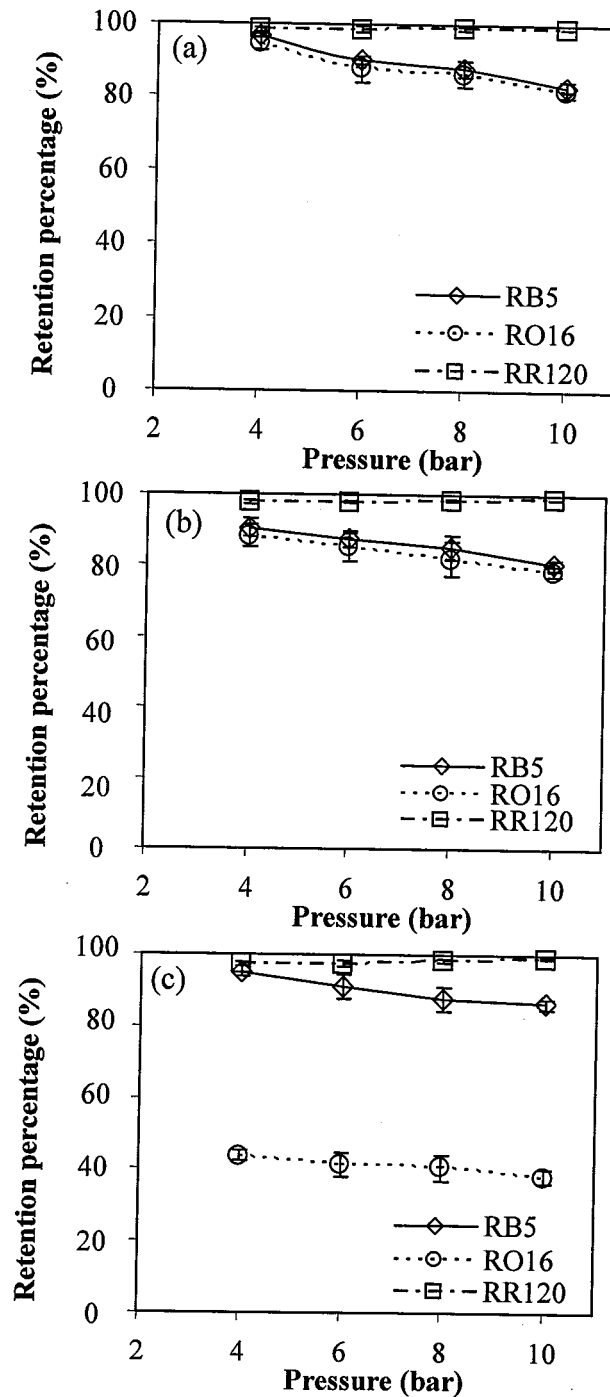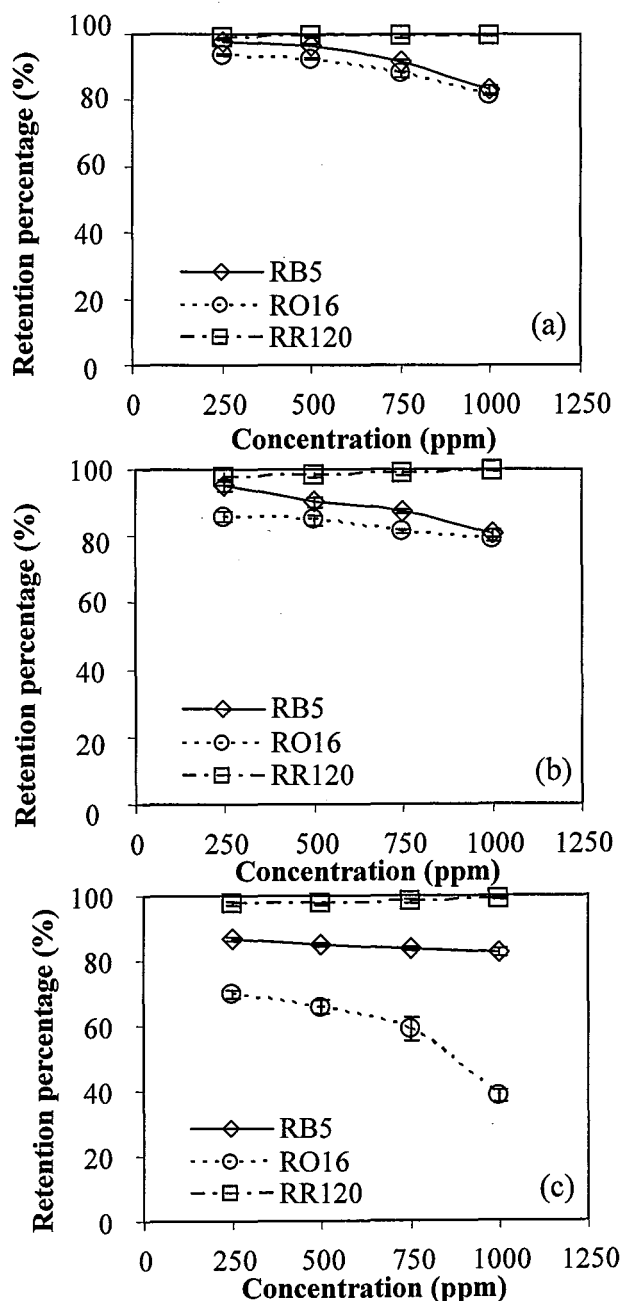

Fig. 23. Retention of RR120, RB5 and RO16 dyes solution with different concentrations at 10 bar using (a) A000/Si (b) A025/Si and (c) A050/Si membrane.

It is important to understand the influence of concentration on the separation performance since the purpose of NF is to concentrate the effluent. In general, it is observed that the rejection of RR120 is the highest, followed by RB5 and RO16. The effect of dye feed concentration on the removal of RR120 is insignificant. However, the permeate quality reduces when feed concentration of smaller dyes (RB5 and RO16) increases. This is possibly due to the rising of concentration polarization effect. Concentration polarization is usually more severe in higher concentrated feed solution (Mulder, 1996).

In dye separation, the permeability of membrane is another important rating besides rejection. Although water permeability of membranes with bimodal porous structure is considerably high, the permeate flux in dye separation may reduce due to concentration polarization and fouling. This study aims to examine the changes of permeate flux when organic ions, RB5 is added into the feed solution. It is also interesting to study the effect of pressure and dye concentration on the permeate flux of bi-layered membranes with different pore volumes. Unlike the rejection, the permeate flux of membranes in dye separation varies with time. The variation of permeate fluxes for water and dye solution is presented in Fig. 24. It is clear from the graphs that A050/Si and A025/Si show higher flux in dye separation compared to A000/Si membrane, which proves permeability enhancement using bimodal porous layer. It is also observed that the flux is improved for higher operating pressure. This is because the driving force across the membrane increases and this leads to augmentation of permeate flux. However, dye solution flux is lower than the corresponding pure water flux ($t = 0$ hr); which can be related to the presence of organic solute. The observation may be attributed to a combination of concentration polarization, adsorption and osmotic pressure effect (Koyuncu et al., 2004a). Operated at same pressure (10 bar), the flux reduction is more severe in the dye solution with high concentration as shown in Fig. 25.

The observation can be related to more serious concentration polarization, adsorption and osmotic pressure in further concentrated of dye solution (Wiesner and Aptel, 1996). Over time, the decline of fluxes approach steady state as shown in Fig. 24 and Fig. 25. The steady state conditions attain a further decrease after running for 3 hr, which is not studied in this work. Such continuous flux decline is the result of membrane fouling such as cake formation which is complex and difficult to describe theoretically. In this study, the observed permeate fluxes at steady state is possibly diminished by osmotic pressure, polarization phenomena and adsorption. The osmotic pressure can be calculated according to Van't Hoff's equation with assumption that concentration polarization is limited by stirring. The osmotic pressure for each experiment in Fig. 24 and Fig. 25 is calculated in order to predict flux decline as summarized in Table 8. The osmotic pressure raises with the increment of dye concentration as expected. However, the flux decline caused by osmotic flux is negligible. The estimated permeate flux is far from the observed flux indicating that the flux decline is less affected by osmotic pressure.
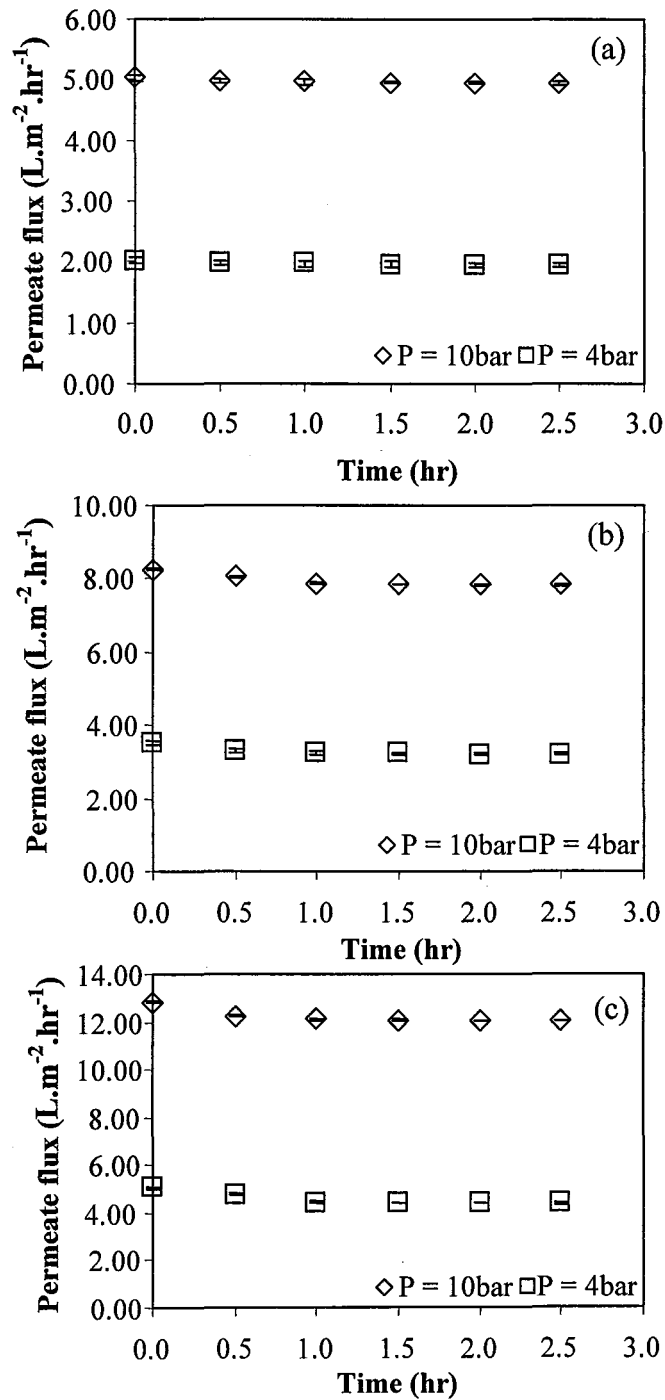
Fig. 24. Permeate flux versus time for RB5 aqueous solution with feed concentration of 1000 ppm separated using (a) A000/Si, (b) A025/Si and (c) A050/Si at 4 bar and 10 bar.
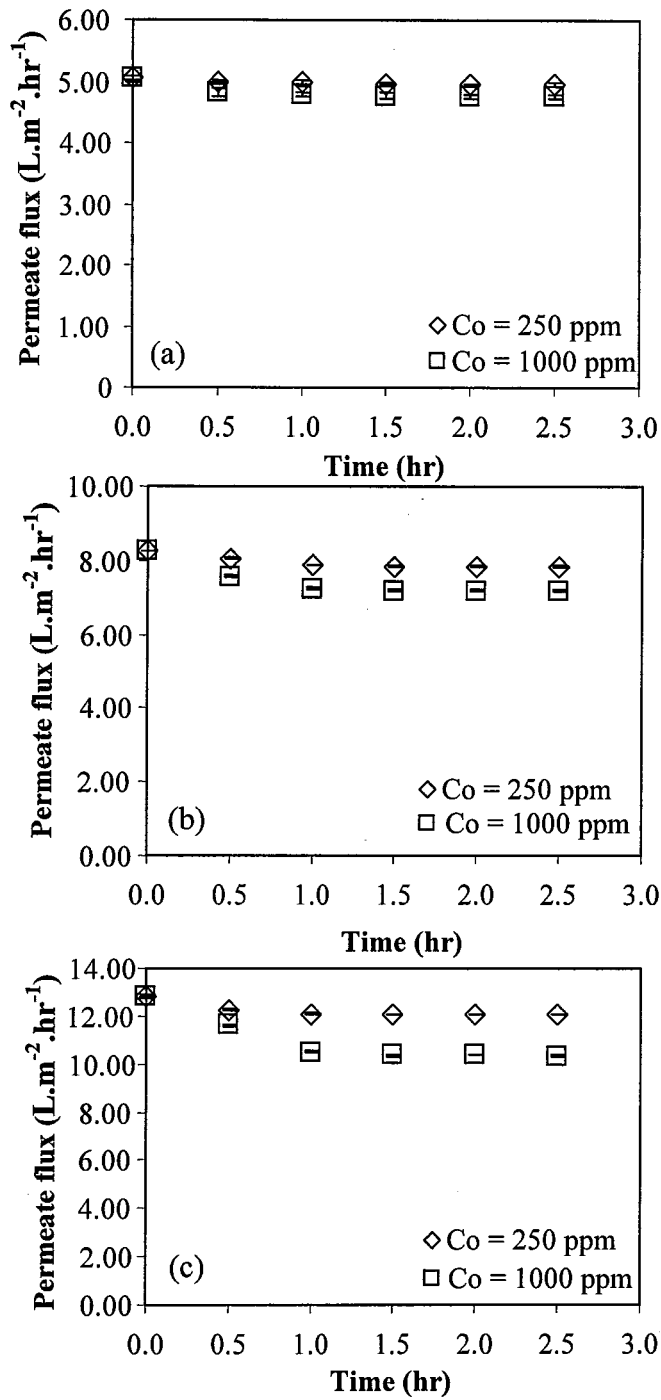
Fig. 25. Permeate flux versus time for RB5 aqueous solution with different feed concentrations separated using (a) A000/Si, (b) A025/Si and (c) A050/Si at 10 bar.

Table 8 Estimated osmotic pressure and predicted permeate flux

Membrane	ΔP (bar)	$C_{F, dye}$ (ppm)	$\Delta\pi_{dye}$ (bar)	J_w (L.m^{-2}.hr^{-1})	J_{estm} (L.m^{-2}.hr^{-1})	J_{obs} (L.m^{-2}.hr^{-1})
	4	250	0.0028	1.98	1.96	1.95
A000/Si	10	250	0.0072	4.95	4.93	4.95
	10	1000	0.1683	4.95	4.90	4.76
	4	250	0.0305	3.32	3.28	3.21
A025/Si	10	250	0.0303	8.26	8.24	7.84
	10	1000	0.1006	8.26	8.18	7.18
	4	250	0.0297	5.14	5.10	4.38
A050/Si	10	250	0.0270	12.84	12.81	12.06
	10	1000	0.1030	12.84	12.71	10.34

J_w= Permeate flux of pure water; J_{estm}= Estimated permeate flux; J_{obs}= Observed permeate flux

In a dead end stirred cell, polarization is unavoidable and it can only be reduced by stirring (Scott, 1998). The dye concentration gradually increases at membrane surface as a result of dye retention. Such a concentration build-up generates a diffusive flow back to the bulk of the feed until the establishment of steady-state as shown in Fig. 24 and Fig. 25. In addition, the dye concentration in the permeate stream shows the dye passages from feed side to permeate. Therefore, dye molecules might have caused adsorptive pore fouling in the membranes. According to the kinetic model proposed by Wiesner and Aptel (1996), the permeate flux which is affected by concentration polarization and adsorption can be predicted using Equation 5.

The linear form of Equation 4.21 is

$$\ln(J_t - J_{ss}) = \ln B - Kt \tag{5}$$

where J is the permeate flux (L.m^{-2}.bar^{-1}), J_{ss} (L.m^{-2}.bar^{-1}) is the steady-state flux, B (L.m^{-2}.bar^{-1}) is the constant, K (hr^{-1}) is the time constant and t is the time. The observed permeate fluxes fit into the kinetic model adequately with relative high R^2 as shown in Table 9. The rate constant increased with increasing dye concentration, pressure and secondary pore volume of membranes.

Table 9 Fitting observed permeate fluxes to kinetic model

Membrane	ΔP (bar)	$C_{F, dye}$ (ppm)	k (hr^{-1})	B (L.m^{-2}.hr^{-1})	R^2
	4	250	1.25	0.06	0.9836
A000/Si	10	250	1.40	0.08	0.9648
	10	1000	2.14	0.24	0.9782
	4	250	2.20	0.30	0.9910
A025/Si	10	250	2.57	0.53	0.9762
	10	1000	3.18	1.36	0.9862
	4	250	2.50	0.88	0.9622
A050/Si	10	250	2.89	0.82	0.9983
	10	1000	3.29	3.86	0.9549

It is rational to detect synergetic effect of dye concentration and pressure since concentration polarization and adsorption are enhanced by the dye feed concentration and flux in general (Wiesner and Aptel, 1996). The increment of rate constant from A000/Si to A025/Si and followed by A050/Si reveals the disadvantages of secondary pores. Besides resulting in more severe concentration polarization with increasing permeability, the secondary pores also promote the adsorption of dye molecules on the primary pores. Though, the weakness of bimodal porous membranes can be improved using modules such as tubular module for future application.

Besides dyes, it is important to understand membrane characteristics in inorganic ions separation especially *NaCl*. This is because salt is the major component in common textile wastewater (Allegre *et al.*, 2006). Silica/γ-alumina membranes with charged surface provide a rigid ceramic structure which is able to retain the small salt ions. Unlike dye molecules in the previous study, the hydrated size of Na^+ (0.72 nm) and Cl^- ions (0.66 nm) (Lia *et al.*, 2004, Lin and Murad, 2001) are much smaller than the pore size of A000/Si, A025/Si and A050/Si membranes. Retention of *NaCl* is easily affected by variables such as concentration, pressure and pH. The effect of these variables on salt rejection and permeate flux are studied in this section. The retention of *NaCl* aqueous solution is measured as a function of pressure for two salt concentrations using different bi-layered membranes. The results of the study are shown in Fig. 26. In general, the salt rejection decreases when the feed salt composition increases. The observation can be explained by the Donnan effect regarding a decrease of membrane surface charge (Tanninen *et al.*, 2007). Besides that, the increment of pressure results in an improvement of *NaCl* retention. This is likely owing to the differences between the salt diffusivity and water permeability through membranes at higher permeate flux (Tanninen *et al.*, 2007). The asymptotic rejection is obtained at driving pressure which is higher than 10 bar.
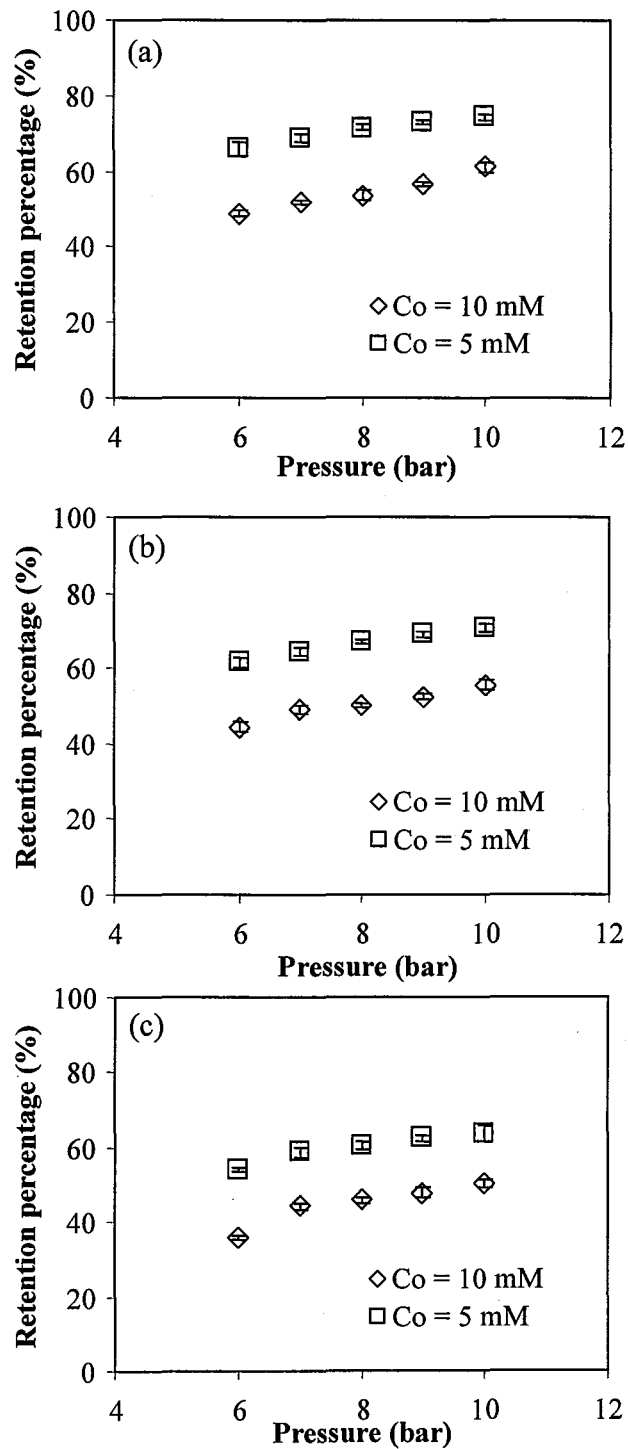
Fig. 26. Salt retention of (a) A000/Si, (b) A025/Si and (c) A050/Si at different pressure for feed solutions with concentration of 5 mM and 10 mM.

The plots of permeate flux versus pressure for salt separation conducted using A000/Si, A025/Si and A050 membranes are illustrated Fig. 27. The permeate flux increases linearly as the applied pressure increases. Despite of the presence of salt in feed solution, the permeate flux is close to the pure water volume flux.
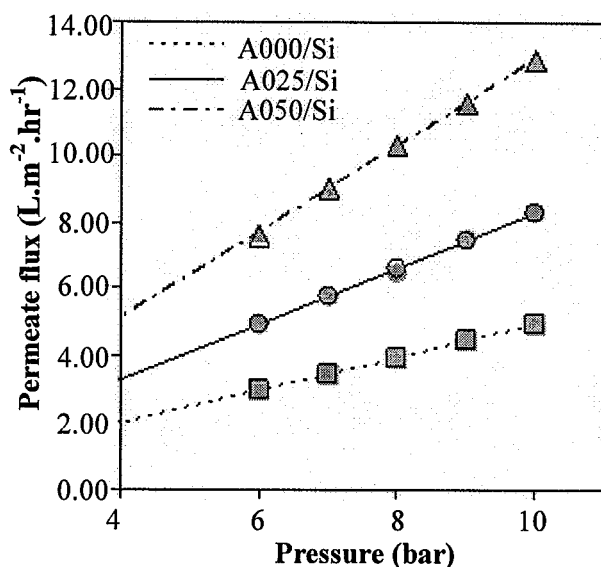
Fig. 27. Permeate flux of (a) A000/Si, (b) A025/Si and (c) A050/Si at different pressure for pure water (lines) and salt feed solutions with concentration of 5 mM (grey markers) and 10 mM (blank markers).

This is probably because the salt concentration at 5 mM and 10 mM is relatively low and the effect of osmotic pressure difference across the membrane is minor (Bowen et al., 1997). Besides that, the stability in flux is one of the advantages of inorganic membranes over organic membranes as they can be operated at high pressures without compaction of open pore structure (Skluzacek et al., 2006). Separation of NaCl at different pH values using silica/γ-alumina membrane has been conducted by Samuel de Lint et al. (2006). In their work, retention of salt is satisfactory in the range of pH 4-10 where silica layer determines retention at pH > 6 and γ-alumina layer determines retention at 4 < pH < 5. Fig. 28 shows such characteristic of silica/γ-alumina membranes with different porous structures. As expected, the separation performance is relatively constant for conventional membrane A000/Si: the retention of the two-layer system over the whole pH range varies between 60 % and 70 %. When γ-alumina with bimodal pore size distribution (A025 and A050) is utilized as intermediate layer, the retention of NaCl reduces with the increment of secondary pore volume. However, the salt retention is reasonably constant except for pH 4. The retention of NaCl is 54 % and 51 % using membrane A025/Si and A050/Si respectively.
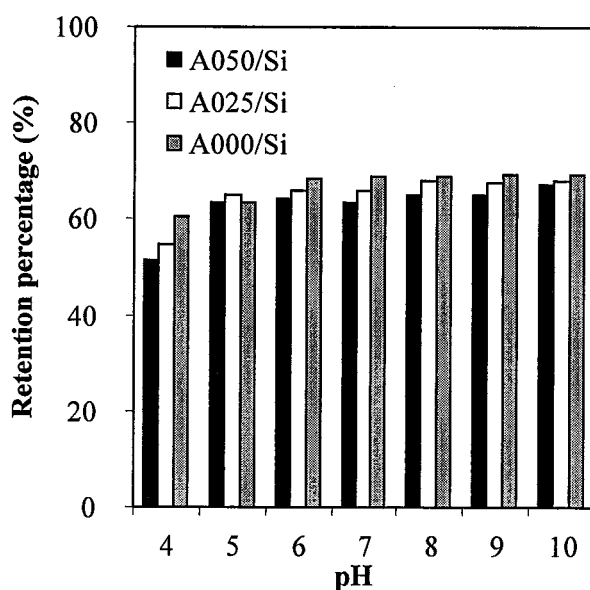
Fig. 28. Mean retention of *NaCl* with concentration of 7.5 mM and various pH values at 10 bar using different membranes.

For salt separation at pH 5 - 9, all membranes show reasonable permeate fluxes which are slightly lower than their respective pure water fluxes (Fig. 29). The negligible reduction of the flux is possibly because that the osmotic pressure difference between the filtrate and the feed solution adjacent to the membrane surface is low at less concentrated salt solutions. At highly acidic and alkaline region, permeate flux of salt separation is unreasonably elevated for the bi-layered membranes especially A050/Si. The observation in Fig. 28 of increasing flux at pH 10 could be due to a poor alkaline stability of the silica membranes. At extremely alkaline stage, dissolution of the top layer possibly happens; resulting in a reduction of silica layer thickness (Nishiyama *et al.*, 2003). Thus, permeate flux for all membranes increase at pH 10. There is likely no increment of pore size as the retention of *NaCl* is well maintained at pH 10. Besides dissolution of the silica layer, the increment in flux at pH 4 might also be caused by the structural changes of the templated silica material. Dobyle and Hodnett (2003) reported that MCM- 48 changed its pore diameter in acidic conditions (pH < 5.4). The fine porous structure disappeared at pH 6.9 and further transformed at pH > 9.1. The morphology changes are likely to influence on the transport properties of the silica layer, causing the poor retention at pH 4 for membranes A025/Si and A050/Si.
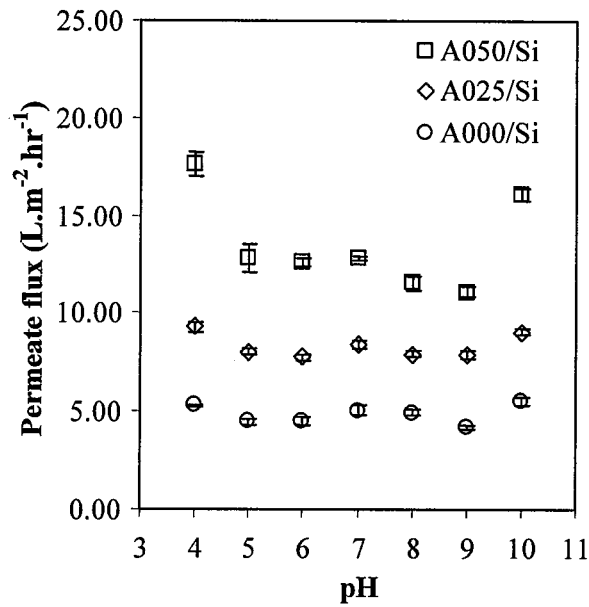
Fig. 36 Permeation flux for *NaCl* separation at 10 bar with feed concentration at 7.5 mM using different membranes.

Besides the average pore radius (r_p) and the ratio of membrane thickness to porosity ($\Delta x/A_k$), the effective volume charge density (X_d) is another vital parameter to describe membrane characteristics in the ions separation. A further analysis of effective volume charge density can be carried out using the salt separation results in order to describe the steric and charge effect upon rejection behavior. The effective volume charge density of membranes is determined for the neutral *NaCl* aqueous solution with different concentrations. The values of effective volume charge density deduced from real retention versus permeate flux curves are given in Table 10.

Table 10 Effective volume charge density X_d for different bi-layered membranes calculated from *NaCl* separation with different feed concentrations at pH 7

Membrane	$C_{F, salt}$ (mM)	X_d (mol/m^3)	R^2
A000/Si	5	-183.56	0.9703
	10	-206.71	0.9712
A025/Si	5	-162.30	0.9526
	10	-184.79	0.9660
A050/Si	5	-139.53	0.9648
	10	-172.55	0.9654

The fitting results are satisfactory as R^2 for each fitting is relatively high. All silica/γ-alumina membranes (A000/Si, A025/Si and A050/Si) possess negatively charged surface in neutral salt solution with concentration of 5 mM. As mentioned before, the silica layer completely determines the membrane retention for pH > 6. Thus, bi-layered membranes only exhibit negative effective volume charge density which is similar with silica membranes (Skluzacek *et al.*, 2007). The magnitude of

effective volume charge density appears to increase with increasing salt feed concentration. This behavior is typical of ceramic membranes and results from an enhanced electrostatic screening leading to an increase of surface ionization (Labbez *et al.*, 2002). It should be also underlined that the effective volume charge density of bi-layered membranes drops when higher secondary pore volume is introduced in γ-alumina layer. This may be related to the reduction of silica density in A025/Si and A050/Si membranes. The exhibited characteristic is a trade-off for the permeability enhancement.

The transport mechanism of ions through the bi-layered membranes with different secondary pore volumes is investigated using two-parameter model of ENP Equation. The transport equations of ions through the membrane account for ionic diffusion and convective flow at electro neutrality condition (Ahmad and Ooi, 2006). The main objective is to identify the changes of transport mechanism which are the controlling factor for monovalent ions rejection. Referring to Equation 3.40, F_i and R_∞ are concentration and pH dependent and can only be obtained through curve-fitting. Fitting the rejection-flux curves with the two-parameter model gives the diffusive and convective parameter for Na^+.

$$J_i = -F_i \Delta C_i + J_v C_{1,0}(1 - R_\infty) \tag{6}$$

The fitted parameters of F_i and R_∞ are summarized in Table 11. The R^2 of each fitting is well acceptable. It is observed that the contribution of diffusive flow increases when secondary pore volume in bi-layered membranes is higher. The value of F_i rises from 3.48 x 10^{-7} to 13.36 x 10^{-7} m/s.

Table 11 Values of F_i and R_∞ for different bi-layered membranes calculated from *NaCl* separation with feed concentration of 5 mM

Membrane	F_i (10^{-7}m/s)	R_∞	R^2
A000/Si	3.48	0.95	0.9976
A025/Si	7.15	0.96	0.9822
A050/Si	13.36	0.93	0.9921

Referring to Table 12, the augmentation is most possibly due to an increment of membrane porosity which is caused by the silica density reduction.

Table 12 Effect of membrane properties on diffusive and convective flow (Ahmad and Ooi, 2006)

Membrane properties	Diffusive contribution	Convective contribution	Response of Γ
Thickness increased	Decreased	Increased	Decreased
Thickness decreased	Increased	Decreased	Increased
Porosity increased	Increased	Decreased	Increased
Porosity decreased	Decreased	Increased	Decreased
Pore size increased	Decreased	Increased	Decreased
Pore size decreased	Increased	Decreased	Increased

This is because membrane thickness and pore size of silica layer rises from A000/Si membrane to A050/Si membrane as discussed before. For convective flow, the increment of parameter R_∞ for A025/Si membrane compared to A000/Si membrane is insignificant. However, there is a small reduction of R_∞ value for A050/Si membrane indicating greater convective flow. The observation is reasonable as A050/Si membrane is the thickest membrane with enlarged pore size.

3.4 RSM for NF of Dye and Salt Mixture in Aqueous Solution

RSM adopts both mathematical and statistical techniques for modeling and analysis of problems in which responses of interest are influenced by several variables. In Section B.4, RSM with CCD is performed accordance with Table 13. The main objective is to study influence of common operating conditions on the quality and quantity of permeate when A025/Si membrane is applied in the NF of dye-salt-water mixture.

Table 13 CCD arrangement and responses for NF of dye and salt mixture in aqueous solution

Run	Factor					Response		
	A	B	C	D	E	Y_1	Y_2	Y_3
	Temperature	$C_{F, dye}$	$C_{F, salt}$	pH	Pressure	R_{dye}	R_{salt}	Flux
	(°C)	(g/L)	(g/L)		(bar)	(%)	(%)	(L.m^{-2}.hr^{-1})
1	25.0	1	80	5	5.0	91.43	11.73	3.72
2	25.0	3	20	5	5.0	94.69	16.32	3.82
3	25.0	3	20	9	10.0	97.89	60.45	7.45
4	25.0	1	80	9	10.0	94.11	29.81	5.45
5	37.5	2	50	7	7.5	94.87	44.32	6.57
6	25.0	3	80	5	10.0	98.15	27.88	6.45
7	50.0	3	20	5	10.0	98.88	58.23	13.88
8	37.5	1	50	7	7.5	92.88	45.28	7.10
9	25.0	2	50	7	7.5	95.12	42.78	4.89
10	50.0	3	80	9	10.0	98.22	26.34	12.15
11	50.0	1	80	9	5.0	91.45	12.34	6.35
12	25.0	3	80	9	5.0	94.68	10.93	3.65
13	50.0	1	20	5	5.0	91.45	20.38	7.26
14	37.5	2	50	7	7.5	93.95	43.26	6.66
15	50.0	3	20	9	5.0	95.75	16.45	6.85
16	37.5	2	50	5	7.5	95.36	43.76	6.63
17	37.5	2	50	7	7.5	94.75	44.01	6.82
18	37.5	3	50	7	7.5	97.27	39.87	6.83
19	25.0	1	20	5	10.0	94.12	64.23	7.98
20	37.5	2	80	7	7.5	94.67	25.73	5.56
21	37.5	2	50	7	5.0	93.65	14.75	5.78
22	50.0	1	20	9	10.0	94.23	65.23	13.34
23	25.0	1	20	9	5.0	91.20	19.76	3.88
24	50.0	3	80	5	5.0	95.46	10.93	6.30

Table 13 Continued

Run	Factor					Response		
	A	B	C	D	E	Y_1	Y_2	Y_3
	Temperature ($^{\circ}$C)	$C_{F, dye}$ (g/L)	$C_{F, salt}$ (g/L)	pH	Pressure (bar)	R_{dye} (%)	R_{salt} (%)	Flux (L.m^{-2}.hr^{-1})
25	37.5	2	50	7	10.0	95.44	43.65	10.34
26	50.0	2	50	7	7.5	94.65	44.25	9.12
27	37.5	2	50	9	7.5	94.07	40.63	6.72
28	37.5	2	20	7	7.5	94.32	48.75	6.89
29	50.0	1	80	5	10.0	93.89	29.38	12.03

$C_{F, dye}$ = Feed concentration of dye; $C_{F, s}$ = Feed concentration of salt; R_{dye}= Retention of dye; R_{salt}= Retention of salt

As shown in Table 13, CCD is composed of five factors: temperature (A), feed concentration of dye (B), feed concentration of salt (C), pH (D) and pressure (E). The range of factors is selected based on previous literatures and they are common operating conditions for textile wastewater treatment. The responses which are of interest in this study are the percentage retention of dye (Y_1), the percentage retention of salt (Y_2), and the permeate flux (Y_3). Simple linear model and quadratic models are used to represent the significant effect of the operational conditions on the interested responses. It is of course unlikely that a polynomial model will be a reasonable approximation of the true functional relationship over the entire space of the independent variable. However, they usually work well for a relatively small region. The eventual objective of this study is to determine the optimum operating conditions for the newly developed membrane using these models which is difficult to be accomplished via one-factor-at-a-time strategy. The optimum operational conditions for the improved silica/γ-alumina membrane (A025/Si) in the NF of dye-salt-water mixture are important for its future application in textile wastewater treatment. The information leads the module selection and separation system design rapidly and efficiently along a path of improvement toward optimum condition.

The rejection of dye achieves more than 90 % for all operating conditions and feed concentrations as shown in Table 13. This is because the molecular weight of dye molecule (MW for RR120 = 1469.98 Da) is much bigger than MWCO of membrane A025/Si (400 Da) and the retention is strongly controlled by a sieving mechanism (Akbari et al., 2002). However, the percentage of decolorization varied slightly with the test conditions, in the range of 91 – 99 % as shown in Table 13. The lowest dye rejection is observed in Run 23 and the highest dye rejection is observed in Run 7. Without performing statistical analysis, a precise conclusion is difficult to be made on the effect of process variables on the dye rejection.

The Fisher's "F" test is employed for selecting a suitable polynomial model to fit the observed dye rejection. Table 14 shows the results of regression calculation and lack of fit test. The linear model is selected among polynomial models as it possesses the highest F value in the sequential model sum

of squares calculation. The results of regression calculation also indicate the model is highly adequate to represent the observed response. This is because the linear model shows insignificance in the lack of fit test and relatively high R^2 (96.57 %). The results of ANOVA for the linear model are shown in Table 15.

Table 14 Results of sequential model sum of squares and lack of fit test for dye rejection

	Sequential Model Sum of Squares					
Source	Sum of squares	DF	Mean square	F value	Prob > F	Remarks
Mean	260130	1	260130			
Linear	108.69	5	21.74	128.82	< 0.0001	Suggested
2FI	1.07	10	0.11	0.49	0.8649	
Quadratic	0.48	5	0.096	0.33	0.8809	
Cubic	1.73	5	0.35	1.72	0.3473	Aliased
Residual	0.60	3	0.20			
Total	260243	29	8973.90			
	Lack of Fit Test					
Source	Sum of squares	DF	Mean square	F value	Prob > F	Remarks
Linear	3.38	21	0.16	0.64	0.7654	Suggested
2FI	2.31	11	0.21	0.84	0.6600	
Quadratic	1.83	6	0.30	1.22	0.5161	
Cubic	0.10	1	0.10	0.41	0.5895	Aliased
Pure error	0.50	2	0.25			

2FI = 2-factor interaction model; DF = Degree of freedom; F = Fisher; Prob = Probability

Table 15 ANOVA result of response surface linear model for dye rejection

Source	Sum of squares	DF	Mean square	F value	Prob > F	Remarks
Model	108.69	5	21.73	128.82	< 0.0001	Significant
A	0.37	1	0.37	2.21	0.1508	
B	72.92	1	72.92	432.1286	< 0.0001	
C	0.01	1	0.012	0.07	0.7898	
D	0.19	1	0.19	1.11	0.3035	
E	35.20	1	35.20	208.57	< 0.0001	
Residual	3.88	23	0.17			
Lack of fit	3.38	21	0.16	0.64	0.7654	Not significant
Pure error	0.50	2	0.25			
Cor total	112.57	28				

DF = Degree of freedom; F = Fisher; Prob = Probability; Cor total = Corrected Total

The operating temperature (factor A), the feed concentration of *NaCl* (factor C) and the pH of feed solutions (D) are considered giving relatively low effect on the dye rejection using the improved silica/γ-alumina (A025/Si) membrane. This is because probability values of these factors (A, C and D) are more than 0.05. For the NF of aqueous solutions with salt and large dye molecules (> 1000 Da), there were works reported that dye rejection is unaffected by temperature (Koyuncu *et al.*, 2004b), addition of salt (Al-Aseeri *et al.*, 2007) and pH of feed solutions (Ku *et al.*, 2005). Thus, the ANOVA

results are reasonable. On the other hand, the feed concentration of dye (factor B) and the operating pressure (factor E) appear to be the significant factors that affect the variation of dye rejection percentage in this study because their significant probability values (Prob > F) are smaller than 0.0001. The significant factors are further investigated and discussed later.

The insignificant terms in the linear model are removed and the results of ANOVA for the reduced model are summarized in Table 16. ANOVA results shows that the reduced linear model for dye rejection is highly significant in the "F" test. Besides that, the reduced linear model shows insignificant lack of fit. Both calculations show that the reduced linear model is acceptable from the statistical point of view to represent the experimental data of dye rejection. Factor B (feed concentration of dye) and factor E (operating pressure) are significant at 99.99 % confidence level as they present a probability lower than 0.0001. Comparing the feed concentration of dye and the operating pressure, the later factor gives lower effect on the dye rejection since it only contributes 31.27 % of the total variance.

Table 16 ANOVA result of response surface reduced linear model for dye rejection

Source	Sum of squares	DF	Mean square	F value	Prob > F	Remarks
Model	108.12	2	54.06	315.63	< 0.0001	Significant
B	72.92	1	72.92	425.76	< 0.0001	
E	35.20	1	35.20	205.49	< 0.0001	
Residual	4.45	26	0.17			
Lack of fit	3.95	24	0.16	0.66	0.7609	Not significant
Pure error	0.50	2	0.25			
Cor total	112.57	28				

DF = Degree of freedom; F = Fisher; Prob = Probability; Cor Total = Corrected total

The R^2 of the chosen model for decolorization at 96.04 % is quite satisfactory. The plot of the predicted values versus the observed values of dye rejection is shown in Fig. 30. Generally, the rejection of dye can be easily predicted by the model as the observed values are close to predicted values. Adjusted R^2 which is adjusted for the number of terms in the model is also acceptable as the reduced model will be expected to explain about 95.73 % of the variability in new data using two factors. In addition, the predicted R^2 of reduced model (96.04 %) is close to the adjusted R^2 (95.73 %). There is no outlier in the data as the difference is less than 20 %. In conclusion, the reduced linear model is adequate for the observed dye rejection.

The final equations in terms of coded factors (Equation 7) and in terms of actual factors (Equation 8) are shown as below:

$$R_{dye} = 94.71 + 2.0B + 1.40E \tag{7}$$

$$R_{dye} = 86.48963 + 2.01278C_{dye} + 0.55933 Pressure \tag{8}$$

From Equation 7 and 8, the coefficient with the factor represents the effect of the corresponding factor on the dye retention. It is observed that the dye retention is synergistically affected by the operating pressure and the feed concentration of dye. There is no dependency of effect one factor on the level of another factor as the interaction term is absent in the equations.
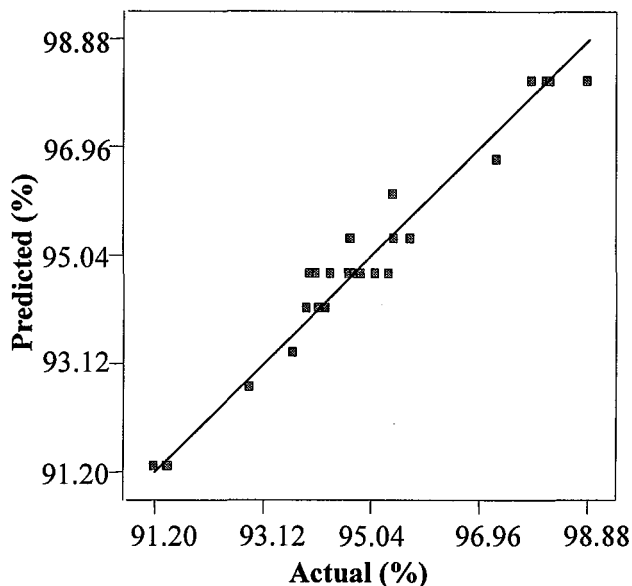
Fig. 30 Predicted and observed values of dye rejection in percentage.

In addition, the experiment results can be interpreted from contour plot (Fig. 31(a)) and 3-D plot (Fig. 31(b)) of response surfaces. The reduced linear model does not contain any interaction terms. Thus, the contours are parallel straight lines and 3-D plot is a plane as the model is first order with only the main effect of factor B (feed concentration of dye) and factor E (pressure). The plots suggest that the dye retention is high if the pressure and the feed concentration of dye is at high level.

Fig. 31 (a) Contour plot and (b) surface response plot for effect of pressure and feed concentration of dye on dye rejection.

The reduced linear model suggests that better color removal can be obtained for higher feed concentration of dye in the dye-salt-water mixture. Al-Aseeri *et al.* (2007) reported similar results but the results were not further explained. Besides that, the model ge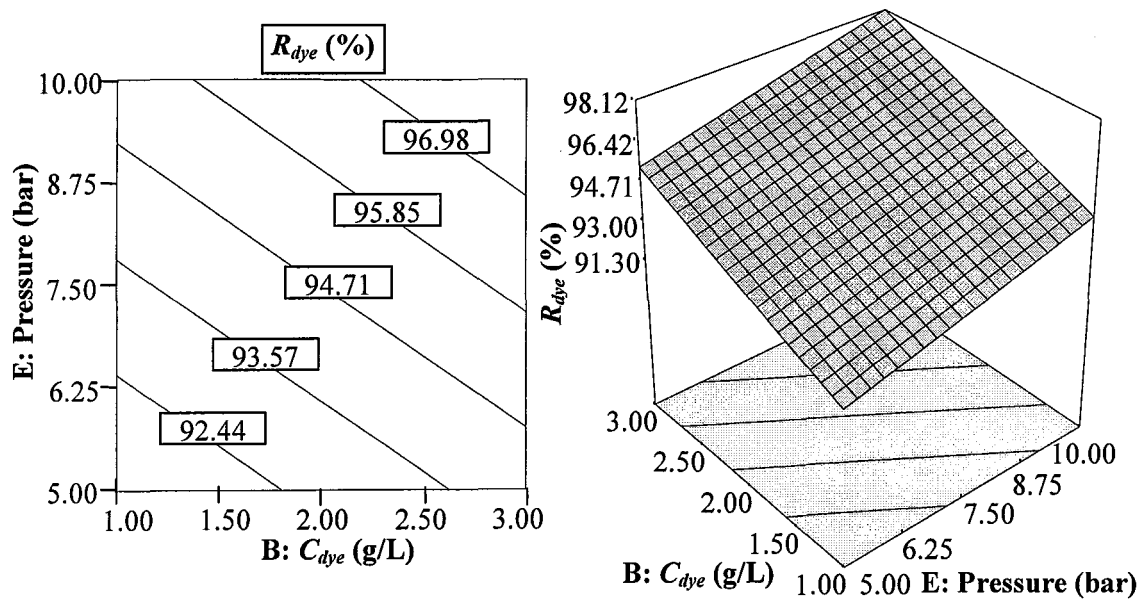nerated using RSM concludes that the dye rejection increases slightly with higher operating pressure. Analogous with the finding of this work, some researchers have reported that increasing the pressure results in a slightly improved dye rejection (Al-Aseeri *et al.*, 2007, Kim *et al.*, 2005, Koyuncu *et al.*, 2004b).

The observation in this section cannot be explained by the usual polarization phenomenon which causes the retention to be lower at higher pressure and feed concentration. This is generally the case with low molecular weight solutes such as salt and small dye molecules (Ku *et al.*, 2005, Mulder, 1996). However, retention can be higher in the case of macromolecular solutes mixture when concentration polarization can have a strong influence on the selectivity (Mulder, 1996). It is obvious that more severe concentration polarization promotes better retention of RR120 due to the high selectivity of dye molecules compared to salt. Concentration polarization phenomenon increases with concentration at membrane surface (C_w) which depends on bulk concentration and flux J as shown in Equation 9 (Mulder, 1996). It is noted that the permeate flux increases with pressure in general membrane separations. Thus, dye concentration and operating pressure synergistically affect the dye rejection as concluded by the reduced linear model.

$$C_w = \frac{C_b \cdot \exp\left(\dfrac{J}{k}\right)}{R_{real} + (1 - R_{real}) \cdot \exp\left(\dfrac{J}{k}\right)} \tag{9}$$

where C_b is concentration of bulk solution (mol/m^3), R_{real} is the real rejection of solute and k is the mass transfer coefficient.

A great variation of salt retention is observed by using NF to separate *NaCl* and dye molecules from aqueous solutions. The salt retention varies between 11 % to 65 % depending on the experimental conditions. This is because salt rejection by silica/γ-alumina membranes is strongly based on electrostatic interactions between the ions in solution and the charged pores of the membrane (Bellona *et al.*, 2004). Without much sieving effect, the percentage of salt rejection is subjected to the separation variables. From Table 13, it can be roughly deduced that the pressure (factor E) and the feed concentration of salt (factor C) affect the rejection of salt from dye-salt-water mixture. However, the significance of other factors such as dye feed concentration, pH and temperature are undetermined by looking at Table 13.

In this section, a quadratic model is recommended for the observed salt retention. Table 17 summarizes the results of regression calculations and lack of fit test which show such recommendation. The quadratic model is significant in sequential model sum of squares and insignificant in the lack of fit test. However, there are only few factors that should be included in the quadratic model as shown in the ANOVA results of the quadratic model (Table 18). The significant

terms include the main effect of dye feed concentration (B), salt feed concentration (C) and pressure (E); quadratic effect of salt feed concentration (C^2) and pressure (E^2); interaction effect of salt feed concentration and pressure (CE). These terms show probability smaller than 0.05 for rejection of the null hypothesis.

Table 17 Results of sequential model sum of squares and lack of fit test for salt rejection

Sequential Model Sum of Squares						
Source	Sum of squares	DF	Mean square	F value	Prob $> F$	Remarks
Mean	34580.59	1	34580.59			
Linear	6046.84	5	1209.37	15.29	< 0.0001	
2FI	739.76	10	73.98	0.89	0.5651	
Quadratic	1051.40	5	210.28	59.29	< 0.0001	Suggested
Cubic	13.13	5	2.62	0.52	0.7578	Aliased
Residual	15.24	3	5.08			
Total	42446.95	29	1463.69			
Lack of Fit Test						
Source	Sum of squares	DF	Mean square	F value	Prob $> F$	Remarks
Linear	1818.94	21	86.62	291.60	0.0034	
2FI	1079.18	11	98.11	330.29	0.0030	
Quadratic	27.78	6	4.63	15.59	0.0615	Suggested
Cubic	14.65	1	14.65	49.32	0.0197	Aliased
Pure error	0.59	2	0.30			

2FI = 2-factor interaction model; DF = Degree of freedom; F = Fisher; Prob = Probability

The insignificant terms are removed from the quadratic model to build the reduced quadratic model for salt rejection. The ANOVA results of the reduced quadratic model are summarized in Table 19. The salt retention is most influenced by factor C (pressure) as this factor contributes 56.83 % of the total variances. Compared to factor C (pressure) and E (feed concentration of salt), factor B (feed concentration of dye) gives the smallest effect on the salt retention. The ANOVA results in Table 19 also show that the fitted second order response surface model is highly significant with F-test value of 205.59 (probability < 0.0001). In the lack of fit test, the reduced quadratic model shows insignificant results which indicates that the model fits the observation well. The reduced quadratic model possesses high R^2 (0.9910). Thus, the predicted salt retention values are close to the observed salt retention values. The good prediction of the reduced quadratic model for salt retention can be observed from Fig. 32. The plot of predicted and observed values are near to the linear line $y = x$. The adjusted R^2 and predicted R^2 for the reduced quadratic model is 0.9886 and 0.9822 respectively. A difference below 0.20 for these values show that the absence of outliers and the adequacy of the model. The coefficients of each term are calculated to form the equations for the salt retention prediction. The formula is written in coded terms (Equation 10) and actual terms (Equation 11). However, it is difficult to determine whether the factor is giving synergistic or antagonistic effect on salt retention. The equations not only involve quadratic terms of some factors but also an interaction term of salt feed

concentration and pressure. The perturbation plot for salt retention (Fig. 33) shows a better picture of the term effect compared to these equations.

Table 18 ANOVA result of response surface quadratic model for salt rejection

Source	Sum of squares	DF	Mean square	F value	Prob > F	Remarks
Model	7838.00	20	391.90	110.50	< 0.0001	Significant
A	0.01	1	0.01	0.002	0.9640	
B	52.47	1	52.47	14.80	0.0049	
C	1895.79	1	1895.79	534.54	< 0.0001	
D	0.04	1	0.04	0.01	0.9138	
E	4098.52	1	4098.52	1155.63	< 0.0001	
A^2	11.33	1	11.33	3.19	0.1117	
B^2	3.58	1	3.58	1.01	0.3442	
C^2	41.76	1	41.76	11.78	0.0089	
D^2	1.67	1	1.67	0.47	0.5114	
E^2	363.09	1	363.09	102.38	< 0.0001	
AB	1.83	1	1.83	0.52	0.4925	
AC	0.05	1	0.05	0.01	0.9086	
AD	0.03	1	0.03	0.01	0.9326	
AE	1.30	1	1.30	0.37	0.5624	
BC	7.52	1	7.52	2.12	0.1835	
BD	0.02	1	0.02	0.01	0.9362	
BE	2.38	1	2.38	0.67	0.4363	
CD	0.65	1	0.65	0.18	0.6796	
CE	725.73	1	725.73	204.63	< 0.0001	
DE	0.25	1	0.25	0.07	0.7981	
Residual	28.37	8	3.55			
Lack of fit	27.78	6	4.63	15.59	0.0615	Not significant
Pure error	0.59	2	0.30			
Cor total	7866.37	28				

DF = Degree of freedom; F = Fisher; Prob = Probability; Cor total = Corrected total

Table 19 ANOVA result of response surface reduced quadratic model for salt rejection

Source	Sum of squares	DF	Mean Square	F value	Prob > F	Remarks
Model	7795.89	6	1299.31	205.59	<0.0001	Significant
B	52.47	1	52.47	16.38	0.0005	
C	1895.79	1	1895.79	591.78	< 0.0001	
E	4098.52	1	4098.52	1279.38	< 0.0001	
C^2	19.55	1	19.55	6.10	0.0217	
E^2	371.64	1	371.64	116.01	< 0.0001	
CE	725.73	1	725.73	226.54	< 0.0001	
Residual	70.48	22	3.20			
Lack of fit	69.88	20	3.49	11.76	0.0812	Not significant
Pure error	0.59	2	0.30			
Cor total	7866.37	28				

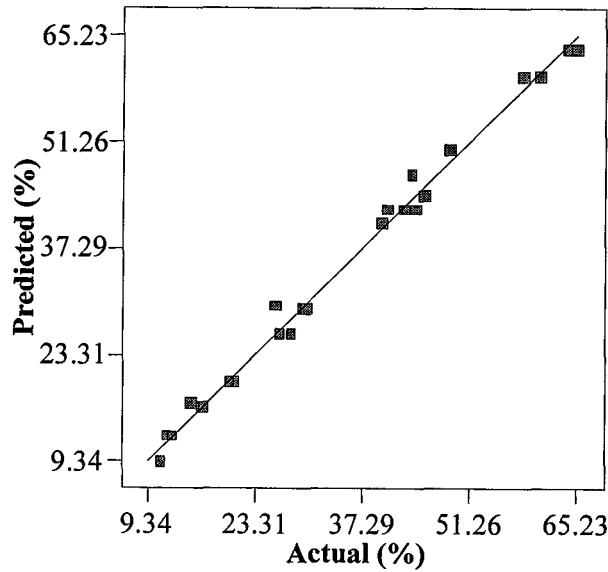DF = Degree of freedom; F = Fisher; Prob = Probability; Cor total = Corrected total

Fig. 32 Predicted and observed values of salt retention in percentage.

$$R_{NaCl} = 42.49 - 1.71B - 10.26C + 15.09 \times 10^{-2.396}C^2 - 10.43E^2 - 6.73CE \qquad (10)$$

$$R_{NaCl} = -116.47760 - 1.70736C_{F,\ dye} + 0.59731C_{F,\ NaCl} + 35.56542(Pressure)$$
$$-2.65911 \times 10^{-3}(C_{F,NaCl})^2 - 1.66931(Pressure)^2 \qquad (11)$$
$$-0.089798(C_{F,\ NaCl})(Pressure)$$

The perturbation plot is helpful in comparing the effect of all the factors at a particular point in the design space. The response is plotted by changing only one factor over its range while holding of the other factors constant. By default, the reference point in the graph is at the midpoint (coded 0) of all the factors as shown in Fig. 33. Steep slopes are found in a factor E (pressure) and C (feed concentration of salt). This observation shows that the salt retention is sensitive to the changes of pressure and salt feed concentration. A relatively flat line in factor B (feed concentration of dye) shows insensitivity of salt removal to the change in dye feed concentration. From Fig. 33, it is remarked that the feed concentration of dye and salt give antagonistic effect on the salt retention while the pressure gives a synergistic effect on the salt retention. However, the plot is like "one factor at a time" experimentation and does not show the effect of interactions. The antagonistic effect of salt concentration on the salt retention percentage can be related to the principle of Donnan equilibrium. Repulsive force of the ceramic membrane (negatively charged) decreases with increasing salt concentration due to higher concentrations of Na^+ cations on the membrane surface. Overcoming the repulsive force also allows more Cl^- anions to pass through the membrane. More salt permeate through the ceramic membrane at higher $NaCl$ feed concentration, and this lowers the salt rejection (Jiraratananon et al., 2000, Tang and Chen, 2002).
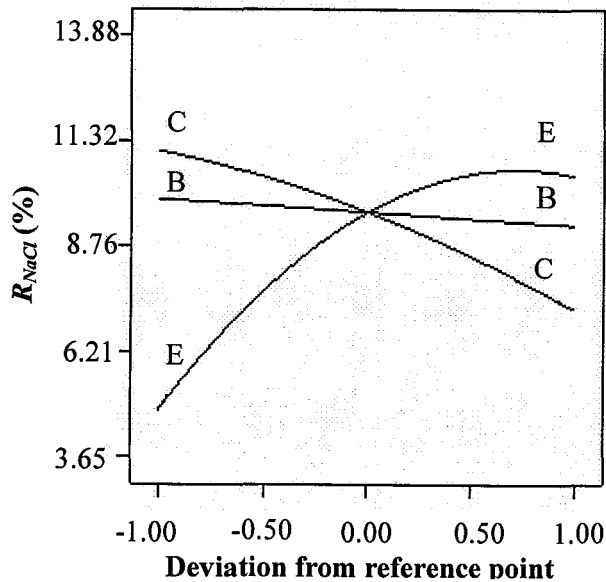
Fig. 33 Perturbation plot for permeate flux.

Specifically, the reduction in salt retention is possibly due to the concentration polarization phenomenon. For aqueous solution with high concentration of salt and dye, the effect of concentration polarization is unavoidable in NF (Koyuncu and Topacik, 2002). Due to the increased solute concentration at the membrane surface, the observed retention will be lower than the real retention. Thus, increasing the concentration of salt and dye in the feed solution results a lower salt retention. The range of dye feed concentration (1 - 3 g/L) is far lower than salt feed concentration (20 – 80 g/L) in the design space. Consequently, the main effect of the dye feed concentration on the salt retention is less significant compared to the feed concentration of salt.

It is noted that the salt rejection improved with increasing flux because the chloride salts retention is enhanced by convection mechanism as flux increases (Bowen and Mohammad, 1998). Pressure is one of the main driving forces for flux so it is reasonable to have positive main effect of pressure on the salt retention. The synergetic effect of pressure on the salt retention, however, is limited by the quadratic effect of pressure. At higher flux, the rejection of salt decreases slightly due to more severe concentration polarization. Besides that, the interaction term of pressure and the feed concentration of salt can be explained by the occurrence of osmotic pressure. Osmotic pressure depends on the difference of salt concentration over the membrane as stated in Van't Hoff equation. The osmotic pressure increases with the salt feed concentration and it results in a lower rejection of salt.

Fig. 34 shows the effect of two factors, pressure and feed concentration of salt when the feed concentration of dye is 2 g/L. As observed from Fig. 34, a combination of high pressure and low salt feed concentration lead to great rejection of salt. The operating pressure should be set higher than 7.5 bar if salt retention higher than 50 % is desired.
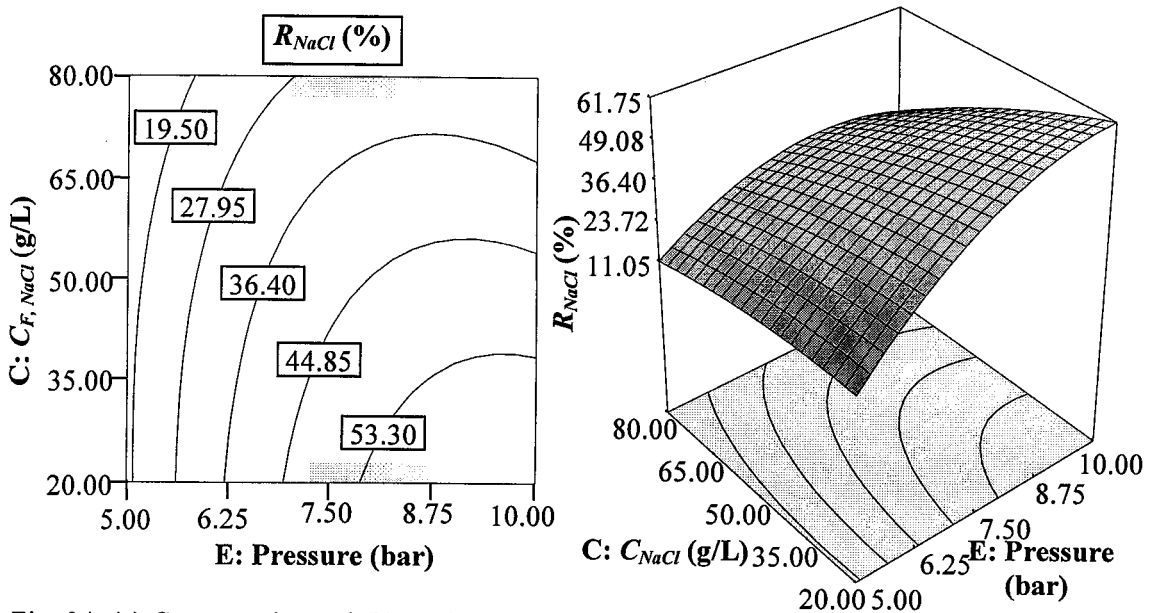
56

Fig. 34. (a) Contour plot and (b) surface response plot for effect of pressure and feed concentration of salt on salt rejection (C_{dye} = 2 g/L).

The effect of dye feed concentration on the salt retention is illustrated in Fig. 35. From Fig. 35, it is obvious that salt retention is strongly affected by the pressure compared to dye feed concentration. This is because variation of salt retention is small even there are changes of dye concentration for pressure higher than 7.5 bar. High salt retention can be achieved at low feed concentration of salt and high pressure.
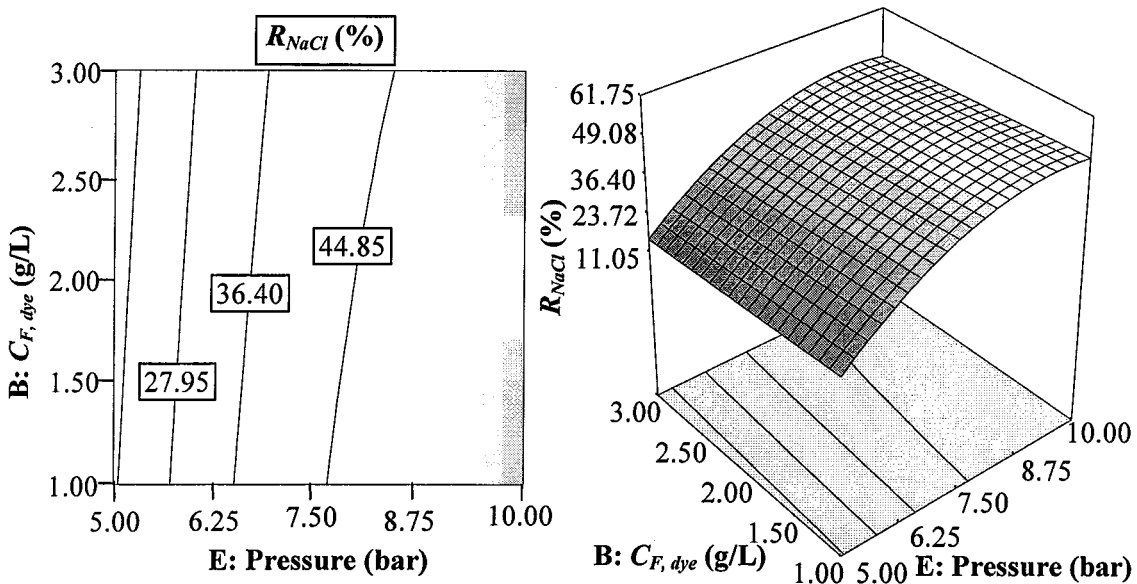

Fig. 35 (a) Contour plot and (b) surface response plot for effect of pressure and feed concentration of dye on salt rejection ($C_{F, NaCl}$ = 50 g/L).

Among the dependent variables, permeate flux is the most sensitive response. This is because the permeate flux is affected by the operating pressure, the viscosity of feed solution, the osmotic pressure, the membrane resistance, the phenomenon of concentration polarization and the membrane fouling. The susceptible characteristic of permeate flux explains the great deviation of the observed permeate flux in Table 13. The difference between the highest flux (13.88 $L.m^{-2}.hr^{-1}$ in Run 7) and the lowest flux (3.65 $L.m^{-2}.hr^{-1}$ in Run 12) is as much as 73.70 %.

In the results of sequential model sum of squares, a quadratic model is advised. A small p-value (Prob > F) indicates that adding interaction terms and quadratic terms into the linear model has improved the model (Table 20). The quadratic model is sufficient to represent to the observed permeate flux as it is insignificant in the lack of fit test. The R^2 of the quadratic model (0.9986) is the highest among the polynomial models, implying a high accuracy for the permeate flux prediction.

Table 5.20 Results of sequential model sum of squares and lack of fit test for permeate flux

Sequential Model Sum of Squares						
Source	Sum of squares	DF	Mean square	F value	Prob > F	Remarks
Mean	1527.52	1	1527.52			
Linear	189.87	5	38.00	47.02	< 0.0001	
2FI	11.74	10	1.17	2.23	0.0879	
Quadratic	6.57	5	1.31	39.61	< 0.0001	Suggested
Cubic	0.18	5	0.04	1.21	0.4664	Aliased
Residual	0.088	3	0.03			
Total	1735.96	29	59.86			
Lack of Fit Test						
Source	Sum of squares	DF	Mean square	F value	Prob > F	Remarks
Linear	18.5418	21	0.88	55.07	0.0180	
2FI	6.800673	11	0.62	38.56	0.0255	
Quadratic	0.233217	6	0.04	2.42	0.3206	Suggested
Cubic	0.055831	1	0.06	3.48	0.2030	Aliased
Pure error	0.032067	2	0.02			

2FI = 2-Factor interaction model; DF = Degree of freedom; F = Fisher; Prob = Probability

In the current design space, the effect of dye feed concentration on the permeate flux is negligible. The ANOVA results of the quadratic model (Table 21) confirm that the p-value (Prob > F) of factor B (the feed concentration of dye) is greater than 0.05 which indicates the insignificance. The rest of the factors (A, C, D and E) show significant main effect on the permeate flux. The significant quadratic terms and interaction terms are C^2, E^2, AE, BE and CE. The insignificant terms are removed from the quadratic model to improve the model precision. However, the BE term shows insignificance in the reduced quadratic model (Table 22). The final quadratic model contains only A, C, D, E, C^2, E^2 AE, BE and CE after further removal of the BE term.

Table 21 ANOVA result of response surface quadratic model for permeate flux

Source	Sum of squares	DF	Mean square	F value	Prob > F	Remarks
Model	208.17	20	10.41	313.89	< 0.0001	Significant
A	88.83	1	88.83	2678.78	< 0.0001	
B	0.004	1	0.004	0.12	0.7376	
C	5.23	1	5.23	157.64	< 0.0001	
D	0.27	1	0.28	8.31	0.0204	
E	95.53	1	95.53	2880.82	< 0.0001	
A^2	0.07	1	0.07	2.08	0.1876	
B^2	0.04	1	0.04	1.20	0.3047	
C^2	0.92	1	0.92	27.75	0.0008	
D^2	0.06	1	0.06	1.95	0.1998	
E^2	3.68	1	3.70	110.93	< 0.0001	
AB	0.001	1	0.001	0.04	0.8503	
AC	0.03	1	0.03	0.80	0.3981	
AD	0.04	1	0.04	1.10	0.3254	
AE	9.60	1	9.60	289.40	< 0.0001	
BC	0.13	1	0.13	4.04	0.0791	
BD	0.16	1	0.16	4.96	0.0566	
BE	0.18	1	0.18	5.54	0.0465	
CD	0.02	1	0.02	0.50	0.5005	
CE	1.43	1	1.43	43.03	0.0002	
DE	0.16	1	0.16	4.68	0.0626	
Residual	0.27	8	0.03			
Lack of fit	0.23	6	0.04	2.42	0.3206	Not significant
Pure error	0.03	2	0.02			
Cor total	208.44	28				

DF = Degree of freedom; F = Fisher; Prob = Probability; Cor total = Corrected total

The ANOVA results of the final quadratic model are summarized in Table 23. The "Lack of Fit F-value" of 3.85 implies the phenomenon lack of fit is not important relative to the pure error therefore the final quadratic model is expected to fit the observed permeate flux well. The plot of predicted and observed permeate flux values is illustrated in Fig. 36. The values is closed to the line y = x as the final quadratic model possesses great R^2 of 0.9945. The final quadratic model is expected to explain new data well since the predicted R^2 achieves 0.9871 which is relatively high. Based on the number of terms in the final quadratic model, the value of adjusted R^2 is calculated at 0.9923. The difference of predicted R^2 and adjusted R^2 is less than 0.20, signifying that the model is adequate and outliers are absent.

Table 22 ANOVA result of response surface reduced quadratic model for permeate flux

Source	Sum of squares	DF	Mean square	F Value	Prob > F	Remarks
Model	207.48	9	23.05	456.51	< 0.0001	Significant
A	88.83	1	88.83	1759.02	< 0.0001	
C	5.23	1	5.23	103.51	< 0.0001	
D	0.28	1	0.28	5.46	0.0306	
E	95.53	1	95.53	1891.69	< 0.0001	
C^2	1.06	1	1.06	21.02	0.0002	
E^2	5.59	1	5.60	110.68	< 0.0001	
AE	9.60	1	9.60	190.03	< 0.0001	
BE	0.18	1	0.18	3.64	0.0718	
CE	1.43	1	1.43	28.25	< 0.0001	
Residual	0.96	19	0.05			
Lack of fit	0.93	17	0.05	3.40	0.2509	Not significant
Pure error	0.03	2	0.02			
Cor total	208.44	28				

DF = Degree of freedom; F = Fisher; Prob = Probability; Cor total = Corrected total

Table 23 ANOVA result of response surface final quadratic model for permeate flux

Source	Sum of squares	DF	Mean square	F value	Prob > F	Remarks
Model	207.30	8	25.91	453.37	< 0.0001	Significant
A	88.83	1	88.83	1554.20	< 0.0001	
C	5.23	1	5.23	91.46	< 0.0001	
D	0.28	1	0.28	4.82	0.0401	
E	95.53	1	95.53	1671.42	< 0.0001	
C^2	1.06	1	1.06	18.57	0.0003	
E^2	5.58	1	5.59	97.79	< 0.0001	
AE	9.60	1	9.60	167.91	< 0.0001	
CE	1.43	1	1.43	24.96	< 0.0001	
Residual	1.14	20	0.06			
Lack of fit	1.11	18	0.06	3.85	0.2259	Not significant
Pure error	0.03	2	0.01			
Cor total	208.44	28				

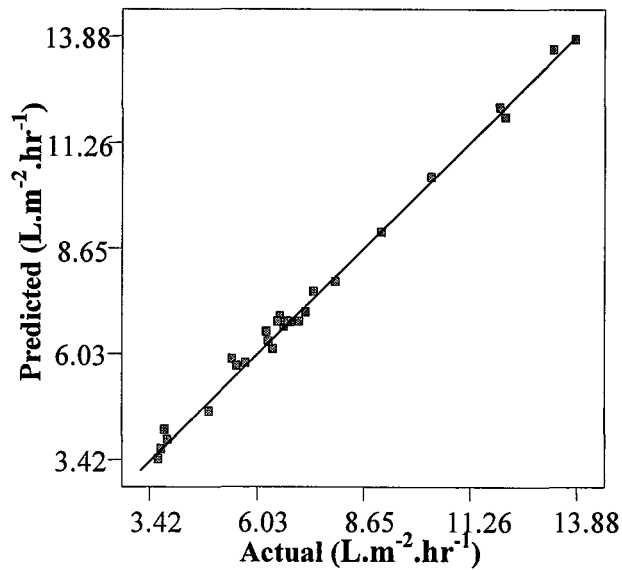DF = Degree of freedom; F = Fisher; Prob = Probability; Cor total = Corrected total

Fig. 36 Predicted and observed values of permeate flux.

Equation 12 and Equation 13 are the equations for the permeate flux prediction using the final quadratic model in coded terms and actual terms respectively. The perturbation plot (Fig. 37) shows that the temperature (factor A) and the pressure (factor E) give synergetic effect on the permeate flux. On the other hand, the feed concentration of salt (factor C) and the pH of feed solution antagonistically affect the permeate flux. It is obvious that the permeate flux is mainly affected by the changes of pressure and temperature. The variation of the feed solution pH in the range 5 to 9 seem to give little effect on the permeate flux. In this pressure driven process, it is reasonable to observe the greatest synergetic effect of pressure on the permeate flux. On the other hand, varying the pH of feed solutions results only in small changes of permeate flux. The increasing of permeate flux is possibly due to structure changes or thickness reduction of silica layer in more acidic solution (Doyle and Hodnett, 2003).

$$Flux = 6.81 + 2.22A - 0.54C - 0.12D + 2.30 \times 10^{-0.55}C^2 + 1.28E^2 + 0.77AE \qquad (12)$$
$$-0.30CE$$

$$Flux = 10.01 - 0.00815(Temperature) + 0.0739C_{Nacl} - 0.06186(pH) - 2.8795(Pressure)$$
$$-6.2 \times 10^{-4}C_{Nacl}^2 + 0.204715(Pressure) + 0.024783(Temperature)(Pressure) \qquad (13)$$
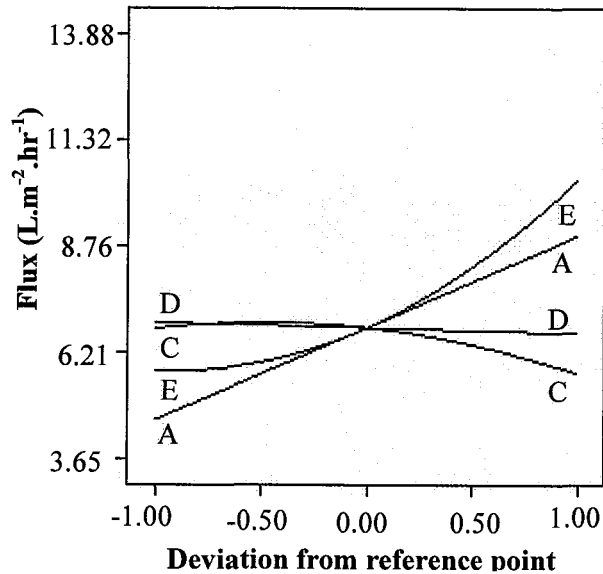$$-3.98 \times 10^{-3}(C_{Nacl})(Pressure)$$

Fig. 37. Perturbation plot for permeate flux.

The dependence of permeate flux on solution temperature has been studied and reported by several previous researchers (Koyuncu et al., 2004b, Ku et al., 2005, Xu and Spencer, 1997a). A possible explanation is that the dynamic viscosity of dye-salt-water mixture declines with elevated solution temperature. The reduction of dynamic viscosity promotes the diffusion rate through the membrane and results in the increment of permeate flux. The effect of temperature on the permeate flux also depends on the level of pressure as temperature increase in a pressurized separation cell.

At higher salt concentration in the feed solutions, the permeate flux decreases significantly. The observation may be due to the growing resistance originating from concentration polarization (Al-Aseeri et al., 2007). Besides that, the opposing effect of interaction term (CE) on the permeate flux is possibly caused by osmotic pressure. Osmotic pressure is unavoidable in this design space as the concentration of salt in the feed solution is relatively high (20 − 80 g/L). The increment of salt concentration causes the rise of osmotic pressure so the effective pressure becomes lower (Koyuncu et al., 2004a). The permeate flux is eventually reduced as the actual driving force becomes lesser. Consequently, the effect of pressure on the permeate flux depends on the salt concentration in the feed solutions.

Contour plots and surface response plots for the predicted permeate flux are illustrated in Fig. 38, Fig. 39 and Fig. 40. All plots show the changes of the permeate flux based on the variation of two factors while other factors are held at middle level. It is observed that high permeate flux is achieved by operating membrane separation of dye-salt-water mixture at high temperature and pressure. The addition of salt into the feed solution results in relatively low permeation which is undesirable. For the range of salt concentration 20 − 80 g/L, it is preferable to set the operating pressure to be higher than 7.5 bar. This is because existence of saddle point as shown in Fig. 38. An operating pressure lower

than 7.5 bar will cause an extremely low permeate flux. From Fig. 40, adjusting pH to acidic phase causes only small increment in permeate flux.
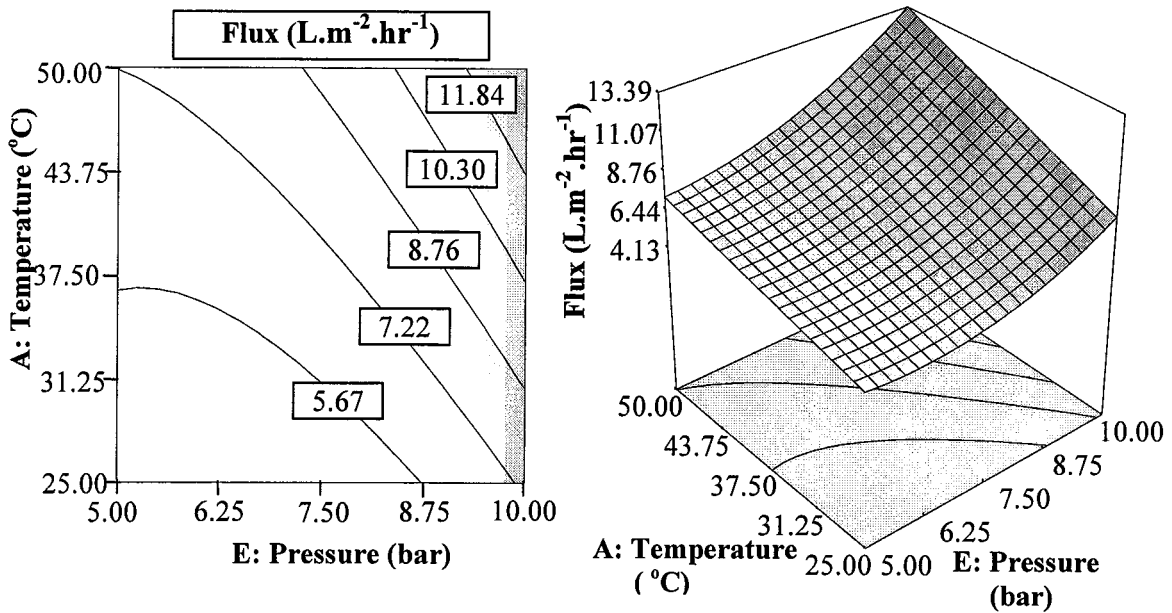

Fig. 38. (a) Contour plot and (b) surface response plot for effect of pressure and temperature on permeate flux ($C_{F,\,NaCl}$ = 50 g/L, pH =7, $C_{F,dye}$ = 2 g/L).
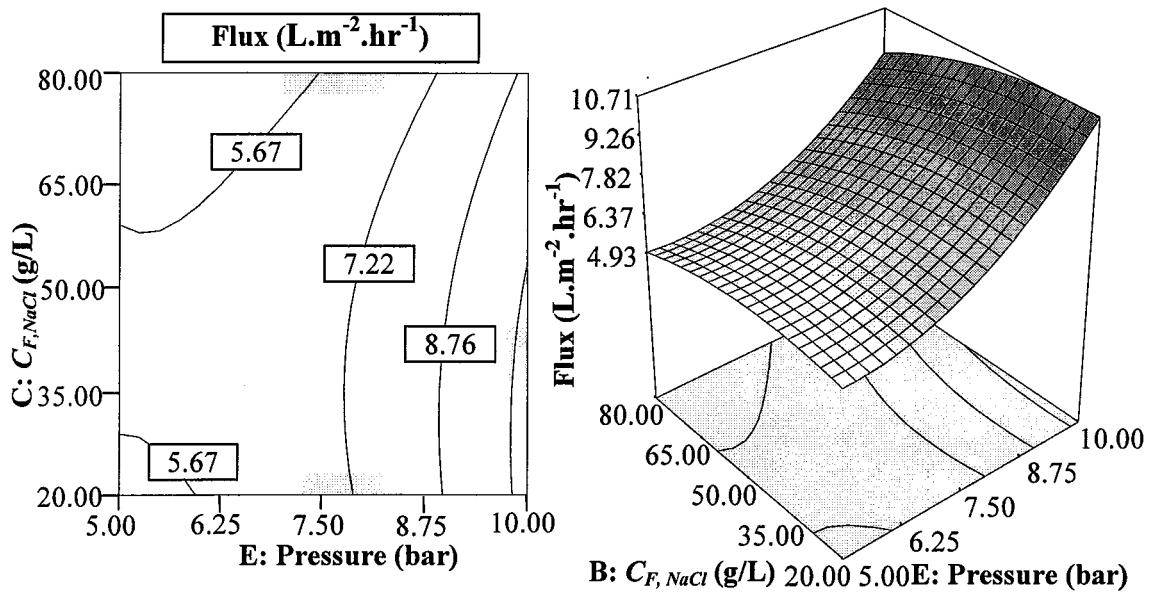

Fig. 39. (a) Contour plot and (b) surface response plot for effect of pressure and feed concentration of salt on permeate flux (temperature = 37.5 °C, pH = 7, $C_{F,dye}$ = 2 g/L).
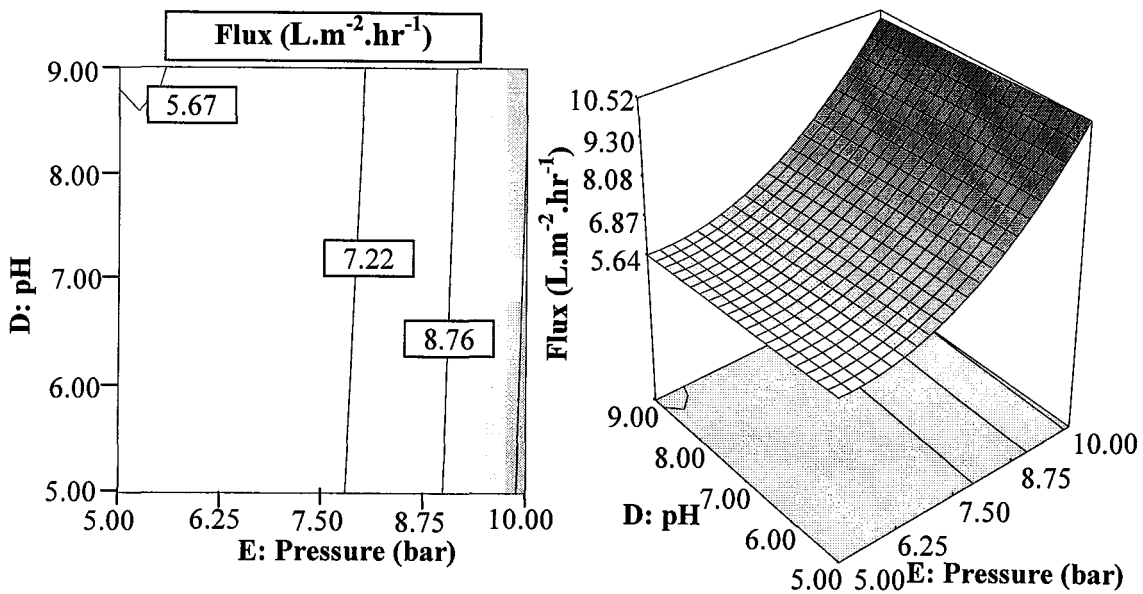
Fig. 40. (a) Contour plot and (b) surface response plot for effect of pressure and on pH on permeate flux (temperature = 37.5 °C, $C_{F, NaCl}$ = 50 g/L, $C_{F,dye}$ = 2 g/L).

From the contour plots (Fig 30, 33, 34, 37, 38 and 39) of dye retention, salt retention and permeate flux, it is obvious that the stationary point does not exist in the common operating range. There is no reason for further search of the stationary points as it is not realistic to operate the separation process out of the common operating conditions. Factors such the salt feed concentration and the dye concentration varies in the range from time to time as they are end-of-pipe waste. A further increment of operating pressure and temperature definitely results in an excessive cost. For achieving long life span of ceramic membrane, the pH of feed solutions should not be adjusted to extremely acidic or alkaline. This study involve a ridge system, in particular, are fairly common.

For multiple responses (R_{dye}, R_{salt} and permeate flux), it is necessary to determine a set of operating conditions that in some sense optimizes all responses or at least keeps them in desired ranges. Overlaying the contour plots for responses is a relatively simple approach to optimize several responses that works well when there are only a few process variables. This straightforward method becomes awkward when there are more than three design variables. A lot of trial and error is often required to decide the constant factors and the levels of factors for achieving the best view of the surface. Therefore, there is practical interest in more formal optimization methods for multiple responses. A popular approach is to formulate and solve the problem as a constrained optimization problem.

In general, NF membranes are used to decolorize the textile wastewater which mainly consists of salts and dyes. The highly concentrated dye solution is later recycled back to the dyeing process to reduce the amount of water mixture. However, the importance of achieving dye retention is lower as the dye rejection is quite stable in the common operating conditions. There are several numerical

techniques that can be used to determine the optimum operation conditions. They are referred to as nonlinear programming methods. The Design Expert software package calculates the desired solution by using a direct search procedure. The possible solutions are shown in Table 24. Using the first solution in Table 24, the experiment (4 replications) is carried out to verify the models in Section 5.5. The average dye retention is 98.65 % and the average salt retention is 25.76 %. Meanwhile, the permeate flux is as high as 12.05 $L.m^{-2}.hr^{-1}$. The experiment result shows that the predicted values are close to the experimental values with error less than 2 %.

Table 24 Solutions for optimum operation conditions of dye-salt-water separation using A025/Si

No.	T (°C)	$C_{F, dye}$ (g/L)	$C_{F, salt}$ (g/L)	pH	P (bar)	R_{dye} (%)	R_{salt} (%)	Flux ($L.m^{-2}.hr^{-1}$)	Desirability
1	50.0	2.94	80.00	5.0	10.0	98.01	26.15	12.12	0.7871
2	50.0	3.00	80.00	5.9	10.0	98.10	26.20	12.00	0.7837
3	50.0	2.94	80.00	5.0	10.0	97.98	26.38	12.02	0.7808
4	43.4	3.00	80.00	5.8	10.0	98.11	26.17	10.44	0.7173
5	50.0	3.00	56.78	5.5	8.7	97.39	42.44	10.70	0.5699
6	50.0	2.98	48.43	6.0	5.0	95.29	15.47	7.30	0.5659
7	50.0	2.98	65.74	5.3	5.0	95.29	12.78	7.06	0.5622
8	50.0	3.00	41.26	9.0	5.0	95.32	16.09	7.13	0.5524
9	50.0	3.00	61.85	8.9	5.0	95.32	13.40	6.94	0.5509
10	50.0	2.98	79.95	5.0	7.0	96.40	26.06	7.55	0.5439

For a high desirability of maximum dye retention, minimum salt retention and maximum flux, the separation process has to be operated at high pressure and temperature. If the feed concentration of salt is low, a lower pressure is required to achieve a low salt retention. However, the permeate flux suffers a great reduction as the prediction flow rate is less than 10 $L.m^{-2}.hr^{-1}$. The optimal conditions which determined using dead-end flow experiments are useful for the future application of A025/Si membrane in the textile wastewater treatment. The information leads the engineers rapidly and efficiently along a path of improvement towards the general vicinity of the optimum condition when other membrane module is employed. Once the region of the optimum has been found, a more elaborate model, such as the extended Spiegler-Kedem model may be employed to ensure further optimization of hydrodynamics conditions.

References

Aguado, J., Escola, J. M., Castro, M. C. & Paredes, B. (2005) Sol-gel synthesis of mesostructured γ-alumina templated by cationic surfactants. *Microporous and Mesoporous Materials,* **83**, 181-192.

Aguilar-Armenta, G. & Díaz-Jiménez, L. (2001) Characterization of the porous structure of two naturally occurring materials through N_2-adsorption (77 K) and gas chromatographic methods. *Colloids and Surfaces A: Physicochemical and Engineering Aspects,* **176**, 245-252.

Ahmad, A. L. & Ooi, B. S. (2006) Characterization of composite nanofiltration membrane using two-parameters model of Extended Nernst-Planck Equation. *Separation and Purification Technology,* **50**, 300-309.

Akbari, A., Remigy, J. C. & Aptel, P. (2002) Treatment of textile dye effluent using a polyamide-based nanofiltration membrane. *Chemical Engineering and Processing,* **41**, 601-609.

Al-Aseeri, M., Bu-Ali, Q., Haji, S. & Al-Bastaki, N. (2007) Removal of Acid Red and sodium chloride mixtures from aqueous solutions using nanofiltration. *Desalination,* **206**, 407-413.

Allegre, C., Moulin, P., Maisseu, M. & Charbit, F. (2006) Treatment and reuse of reactive dyeing effluents. *Journal of Membrane Science,* **269**, 15-34.

Baker, R. W. (2000) *Membrane Technology and Applications.* New York, McGraw-Hill.

Bellona, C., Drewes, J. E., Xu, P. & Amy, G. (2004) Factors affecting the rejection of organic solutes during NF/RO treatment - a literature review. *Water Research,* **38**, 2795-2809.

Boffa, V., Elshof, J. E. t. & Blank, D. H. A. (2007) Preparation of templated mesoporous silica membranes on macroporous α-alumina supports via direct coating of thixotropic polymeric sols. *Microporous and Mesoporous Materials,* **100**, 173-182.

Bowen, W. R., Mohammad, A. W. & Hilal, N. (1997) Characterisation of nanofiltration membranes for predictive purposes - Use of salts, uncharged solutes and atomic force microscopy. *Journal of Membrane Science,* **126**, 91-105.

Buggraaf, T. J. & Keizer, K. (1991) Synthesis of Inorganic Membranes. IN Bhave, R. (Ed.) *Inorganic Membranes Synthesis, Characteristics and Applications.* New York, Chapmen & Hall.

Burggraaf, A. J., Keizer, K. & Van Hassel, B. A. (1989) Ceramic nanostructure materials, membranes and composite layers. *Solid State Ionics,* **32-33**, 771-782.

Choma, J. & Jaroniec, M. (2007) Applicability of classical methods of pore size analysis for MCM-41 and SBA-15 silicas. *Applied Surface Science,* **253**, 5587-5590.

Chowdhury, S. R., Peters, A. M., Blank, D. H. A. & Elshof, J. E. T. (2006) Influence of porous substrate on mesopore structure and water permeability of surfactant templated mesoporous silica membranes. *Journal of Membrane Science,* **279**, 276-281.

Cleveland, C. T., Seacord, T. F. & Zander, A. K. (2002) Standardized membrane pore size characterization by polyethylene glycol rejection. *Journal of Environmental Engineering,* **128**, 399-407.

Cooper, A. R. & Van Derveer, D. S. (1979) Characterization of ultrafiltration membranes by polymer transport measurements. *Separation Science and Technology,* **14**, 551-556.

de Boer, J. H. (1958) The Structure and Properties of Porous Materials. IN Everett, D. H. & Stone, F. S. (Eds.) *Proceedings of the 10th Symposium of the Colston Research Socity.* Butterworths.

De Lint, W. B. S. & Benes, N. E. (2005) Separation properties of γ-alumina nanofiltration membranes compared to charge regulation model predictions. *Journal of Membrane Science,* **248**, 149-159.

Doyle, A. & Hodnett, B. K. (2003) Stability of MCM-48 in aqueous solution as a function of pH. *Microporous and Mesoporous Materials,* **63**, 53-57.

Fu, D. Y. & Tseng, W. J. (2006) Rheology of concentrated SiC particles in silicon alkoxide sols. *Ceramics International,* **32**, 133-136.

Gilbert, R. G. (1995) *Emulsion Polymerization - A Mechanistic Approch,* London, Blackwell Science.

Gregg, S. J. & Sing, K. S. W. (1991) *Adsorption; Surface Area and Porosity,* London, Academic Press.

Honma, I., Zlion, H. S., Kimdn, D. & Endo, D. (2000) Structural control of surfactant-templated hexagonal,cubic, and lamellar mesoporous silicate thin films prepared by spin-casting. *Advanced Materials,* **12**, 1529-1533.

Jaroniec, M. & Solovyov, L. A. (2006) Improvement of the Kruk-Jaroniec-Sayari method for pore size analysis of ordered silicas with cylindrical mesopores. *Langmuir,* **22,** 6757-6760.

Jing, C., Zhao, X. & Tao, H. (2006) An approach to predict the solid film thickness possibly yielded from an alumina sol-gel liquid film. *Surface and Coatings Technology,* **201,** 2655-2661.

Jiraratananon, R., Sungpet, A. & Luangsowan, P. (2000) Performance evaluation of nanofiltration membranes for treatment of effluents containing reactive dye and salt. *Desalination,* **130,** 177-183.

Kim, T.H., Park, C. & Kim, S. (2005) Water recycling from desalination and purification process of reactive dye manufacturing industry by combined membrane filtration. *Journal of Cleaner Production,* **13,** 779-786.

Koyuncu, I. & Topacik, D. (2002) Effect of organic ion on the separation of salts by nanofiltration membranes. *Journal of Membrane Science,* **195,** 247-263.

Koyuncu, I., Topacik, D. & Wiesner, M. R. (2004a) Factors influencing flux decline during nanofiltration of solutions containing dyes and salts. *Water Research,* **38,** 432-440.

Koyuncu, I., Topacik, D. & Yuksel, E. (2004b) Reuse of reactive dyehouse wastewater by nanofiltration: process water quality and economical implications. *Separation and Purification Technology,* **36,** 77-85.

Ku, Y., Lee, P. L. & Wang, W. Y. (2005) Removal of acidic dyestuffs in aqueous solution by nanofiltration. *Journal of Membrane Science,* **250,** 159-165.

Labbez, C., Fievet, P., Szymczyk, A., Vidonne, A., Foissy, A. & Pagetti, J. (2002) Analysis of the salt retention of a titania membrane using the "DSPM" model: Effect of pH, salt concentration and nature. *Journal of Membrane Science,* **208,** 315-329.

Lambert, C. K. & Gonzalez, R. D. (1999) Effect of binder addition on the properties of unsupported γ-Al₂O₃ membranes. *Materials Letters,* **38,** 145-149.

Larbot, A., Alami-Younssi, S., Persin, M., Sarrazin, J. & Cot, L. (1994) Preparation of a γ-alumina nanofiltration membrane. *Journal of Membrane Science,* **97,** 167-173.

Lee, S. Y., Kwon, S. J., Yang, S. M. & Park, S. B. (2005) Preparation of sol-gel driven alumina membrane modified by soaking and vapor-deposition method. *Journal of Membrane Science,* **108,** 97-105.

Leenaars, A. F. M., Keizer, K. & Burggraaf, A. J. (1984) The preparation and characterization of alumina membranes with ultra-fine pores - Part 1 Microstructural investigations on non-supported membranes. *Journal of Materials Science,* **19,** 1077-1088.

Leenaars, A. F. M., Keizer, K. & Burggraaf, A. J. (1985) Structure, permeability, and separation characteristics of porous alumina membranes. IN Sourirajan, S. & Matsuura, T. (Eds) *American Chemical Society Symposium.* Washington.

Lia, L., Dong, J., Nenoff, T. M. & Lee, R. (2004) Reverse osmosis of ionic aqueous solutions on a MFI zeolite membrane. *Desalination,* **170,** 309-316.

Lin, J. & Murad, S. (2001) A computer simulation study of the separation of aqueous solutions using thin zeolite membranes. *Molecular Physics,* **99,** 1175-1181.

Lin, Y. S. (2001) Microporous and dense inorganic membranes: current status and prospective. *Separation and Purification Technology,* **25,** 39-55.

Micromeritics® (1992) ASAP, 2000 User Manual.

Mishra, B. G. & Rao, G. R. (2005) Cerium containing Al- and Zr-pillared clays: Promoting effect of cerium (III) ions on structural and catalytic properties. *Journal of Porous Materials,* **12,** 171-181.

Mulder, M. (1996) *Basic Principles of Membrane Technology,* Dordrecht, Kluwer Academic Publishers.

Nishiyama, N., Saputra, H., Park, D.H., Egashira, Y. & Ueyama, K. (2003) Zirconium-containing mesoporous silica Zr-MCM-48 for alkali resistant filtration membranes. *Journal of Membrane Science,* **218,** 165-171.

Padmaja, P., Anilkumar, G. M., Mukundan, P., Aruldhas, G. & Warrier, K. G. K. (2001) Characterisation of stoichiometric sol-gel mullite by fourier transform infrared spectroscopy. *International Journal of Inorganic Materials,* **3,** 693-698.

Pena-Alonso, R., Tellez, L., Tamayo, A., Rubio, F., Rubio, J. & Oteo, J. L. (2007) Silicon-titanium oxycarbide glasses as bimodal porous inorganic membranes. *Journal of the European Ceramic Society,* **27**, 969-973.

Peterson, R. A., Hill, C. G. & Anderson, M. A. (1990) Permselectivity characteristics of supported ceramic alumina membranes. *Separation Science and Technology,* **25**, 1281-1293.

Sabde, A. D., Trivedi, M. K., Ramachandhran, V., Hanra, M. S. & Misra, B. M. (1997) Casting and characterization of cellulose acetate butyrate based UF membranes. *Desalination,* **114**, 223-232.

Samuel de Lint, W. B., Zivkovic, T., Benes, N. E., Bouwmeester, H. J. M. & Blank, D. H. A. (2006) Electrolyte retention of supported bi-layered nanofiltration membranes. *Journal of Membrane Science,* **277**, 18-27.

Sangwichien, C., Aranovich, G. L. & Donohue, M. D. (2002) Density functional theory predictions of adsorption isotherms with hysteresis loops. *Colloids and Surfaces A: Physicochemical and Engineering Aspects,* **206**, 313-320.

Santos, J. L. C., de Beukelaar, P., Vankelecom, I. F. J., Velizarov, S. & Crespo, J. G. (2006) Effect of solute geometry and orientation on the rejection of uncharged compounds by nanofiltration. *Separation and Purification Technology,* **50**, 122-131.

Scott, K. (1998) Introduction to Membrane Separations. *Handbook of Industrial Membranes.* Second ed. Oxford, Elsevier Advanced Technology.

Sekulic, J., Ten Elshof, J. E. & Blank, D. H. A. (2004) A microporous titania membrane for nanofiltration and pervaporation. *Advanced Materials,* **16**, 1546-1550.

Sigma-Aldrich (2007) [Online], [Accessed 5th November 2007]. Available from World Wide Web: http://www.sigmaaldrich.com/Area_of_Interest/Asia_Pacific_Rim/Malaysia.html

Skluzacek, J. M., Isabel Tejedor, M. & Anderson, M. A. (2006) An iron-modified silica nanofiltration membrane: Effect of solution composition on salt rejection. *Microporous and Mesoporous Materials,* **94**, 288-294.

Skluzacek, J. M., Tejedor, M. I. & Anderson, M. A. (2007) NaCl rejection by an inorganic nanofiltration membrane in relation to its central pore potential. *Journal of Membrane Science,* **289**, 32-39.

So, J. H., Yang, S. M. & Park, S. B. (1998) Preparation of silica-alumina composite membranes for hydrogen separation by multi-step pore modifications. *Journal of Membrane Science,* **147**, 147-158.

Szetu, J. L., Frost, R. L., Kloprogge, J. T., Russell, S. C. & Martens, W. (2000) Dehydration and dehydroxylation of alumina gels prepared from tri-sec-butoxyaluminium modified with short chain aliphatic acids. *Thermochimica Acta,* **362**, 37-48.

Takahashi, R., Sato, S., Sodesawa, T. & Yabuki, M. (2001) Silica-alumina catalyst with bimodal pore structure prepared by phase separation in sol-gel process. *Journal of Catalysis,* **200**, 197-202.

Tang, C. & Chen, V. (2002) Nanofiltration of textile wastewater for water reuse. *Desalination,* **143**, 11-20.

Tanninen, J., Manttari, M. & Nystrom, M. (2007) Effect of electrolyte strength on acid separation with NF membranes. *Journal of Membrane Science,* **294**, 207-212.

Tsai, C.Y., Tam, S.Y., Lu, Y. & Brinker, C. J. (2000) Dual-layer asymmetric microporous silica membranes. *Journal of Membrane Science,* **169**, 255-268.

Tsuru, T., Shintani, H., Yoshioka, T. & Asaeda, M. (2006) A bimodal catalytic membrane having a hydrogen-permselective silica layer on a bimodal catalytic support: Preparation and application to the steam reforming of methane. *Applied Catalysis A: General,* **302**, 78-85.

Uhlhorn, R. J. R., Huis In't Veld, M. H. B. J., Keizer, K. & Burggraaf, A. J. (1989) High permselectivities of microporous silica-modified γ-alumina membranes. *Journal of Materials Science Letters,* **8**, 1135-1138.

Vickreva, O., Kalinina, O. & Kumacheva, E. (2000) Colloid crystal growth under oscillatory shear. *Advanced Materials,* **12**, 110-112.

Wiesner, M. R. & Aptel, P. (1996) Mass Transport and Permeate Flux and Fouling in Pressure-Driven Processes. IN Mallevialle, J., Odendaal, P. E. & Wiesner, M. R. (Eds.) *Water Treatment Membrane Processes.* New York, McGraw-Hill.

Xu, X. & Spencer, H. G. (1997a) Dye-salt separations by nanofiltration using weak acid polyelectrolyte membranes. *Desalination,* **114**, 129-137.

Yoshino, Y., Suzuki, T., Nair, B. N., Taguchi, H. & Itoh, N. (2005) Development of tubular substrates, silica based ,membranes and membrane modules for hydrogen separation at high temperature. *Journal of Membrane Science,* **267**, 9-17.